

Power System Oscillatory Behaviors:

Sources, Characteristics, & Analyses

May 2017
Version 1.0

Disclaimer

This report was prepared as an account of work sponsored by an agency of the United States Government. Neither the United States Government nor any agency thereof, nor any of their employees, makes any warranty, express or implied, or assumes any legal liability or responsibility for the accuracy, completeness, or usefulness of any information, apparatus, product, or process disclosed, or represents that its use would not infringe privately owned rights. Reference herein to any specific commercial product, process, or service by trade name, trademark, manufacturer, or otherwise does not necessarily constitute or imply its endorsement, recommendation, or favoring by the United States Government or any agency thereof. The views and opinions of authors expressed herein do not necessarily state or reflect those of the United States Government or any agency thereof.

Acknowledgments

This paper was written by Jim Follum (Pacific Northwest National Laboratory [PNNL]), Frank Tuffner (PNNL), Luke Dosiek (Union College), and John Pierre (University of Wyoming). This effort was supervised and managed by Eric S. Andersen, PMP, with PNNL.

Funding was provided by the Office of Electricity Delivery and Energy Reliability, United States Department of Energy.

The authors would like to thank Dr. Ning Zhou of Binghamton University for his helpful discussion and review of this document. We also acknowledge the many members of the Western Electricity Coordinating Council's Joint Synchronized Information Subcommittee (WECC JSIS) and the North American SynchroPhasor Initiative (NASPI) that have developed much of the theory referenced in this document. For their helpful discussions over the years, we particularly thank Dr. Dan Trudnowski and Dr. Matt Donnelly of Montana Tech, Dr. Mani Venkatasubramanian of Washington State University, Dr. Bernie Lesieutre of the University of Wisconsin-Madison, and Dr. Dmitry Kosterev of Bonneville Power Administration.

About this Document

This document is intended to provide a broad overview of the sources, characteristics, and analyses of natural and forced oscillatory behaviors in power systems. These aspects are necessarily linked. Oscillations appear in measurements with distinguishing characteristics derived from the oscillation's source. These characteristics determine which analysis methods can be appropriately applied, and the results from these analyses can only be interpreted correctly with an understanding of the oscillation's origin. To describe oscillations both at their source within a physical power system and within measurements, a perspective from the boundary between power system and signal processing theory has been adopted. The power system is viewed as a generic system of inputs and outputs without emphasizing swing equations, generator models, etc. Similarly, the analysis methods used in examples have been selected to represent multiple broad classes, rather than to emphasize the performance of specific methods.

Intended for multiple audiences, this document can be used in a variety of ways. Considering each section will provide the reader with the fundamentals needed to understand power system oscillations and begin applying the described methods. Readers uninterested in applying signal processing methods may focus on sections describing oscillation sources and characteristics and skip those discussing analyses. Others with a solid understanding of power systems may focus primarily on content related to modeling and analysis to broaden their perspective. Whatever the case, the authors hope that this document provides the reader with a new and useful perspective on the important topic of power system oscillatory behavior.

Table of Contents

List of Examples	3
List of Figures	4
List of Tables	7
1. Introduction.....	8
2. Background.....	8
2.1. Overview of System Responses	8
2.2. Overview of Measurement-Based System Models	10
2.2.1. State-Space Models.....	11
2.2.2. ARMAX Models.....	13
2.3. Signal Processing Considerations	13
2.4. Simple Model for Example Data Generation.....	16
3. Natural Response Oscillations	17
3.1. Ambient Response.....	17
3.1.1. Sources of Ambient Responses.....	17
3.1.2. Characteristics of Ambient Responses.....	18
3.1.3. Analysis of Ambient Responses	20
3.2. Transient Response	31
3.2.1. Sources of Transient Responses.....	32
3.2.2. Characteristics of Transient Responses	33
3.2.3. Analysis of Transient Responses	35
4. Forced Response Oscillations	41
4.1. Sources of Forced Responses.....	41
4.2. Characteristics of Forced Responses.....	41
4.3. Analysis of Forced Responses.....	51
4.3.1. Detection of Forced Oscillations	51
4.3.2. Identification of Forced Oscillations	55
5. Analysis of Measurements Containing Natural and Forced Responses	56
6. Works Cited	61

List of Examples

Example 1: Least-Squares Estimation of the Electromechanical Modes using Ambient Data	21
Example 2: Nonparametric Spectral Estimation of Ambient Data	26
Example 3: Use of the Spectral Coherence Estimate to Distinguish Between Electromechanical Modes	28
Example 4: Mode Shape Estimation with the Spectral Method	30
Example 5: Analysis of a Transient Response with Prony’s Method.....	35
Example 6: Effect of System Dynamics on a Forced Oscillation’s Characteristics	42
Example 7: Forced Oscillation Shape.....	47
Example 8: Impact of a Forced Oscillation on an “Ambient” Data Analysis	57

List of Figures

Figure 2-1: Typical examples of ambient, transient, and forced responses. The model used to generate this output is described in Section 2.4.	9
Figure 2-2: Region in the z-domain that electromechanical modes tend to occupy for a sampling rate of 60 samples per second.	15
Figure 2-3: Region in the z-domain that electromechanical modes tend to occupy for a reduced sampling rate of 5 samples per second.	15
Figure 2-4: Conceptualization of the simple transfer function model used to generate example data.	16
Figure 3-1: Example white noise input (top) to the example system and resulting ambient noise response from the system (bottom).	18
Figure 3-2: PSD of the example model’s output signal from Area 2 in the base case. The frequency and damping ratio of each of the model’s electromechanical modes are listed next to their associated peaks.	19
Figure 3-3: PSD of the example model’s output signal from Area 2 with changes to the electromechanical modes. The frequency and damping ratio of each of the model’s modes are listed next to their associated peak.	19
Figure 3-4: Input signal \underline{y} and reconstructed signal $Y\hat{\theta}$ from the LS method.	22
Figure 3-5: PSD of the example model’s output signal from Area 1 in the base case. Note that the 0.6 Hz mode is barely observable. See Table 2-1.	25
Figure 3-6: PSD and least-squares spectral estimate for measurements from the example model’s second area.	26
Figure 3-7: Periodogram and PSD of output data from the second area of the example model. .	27
Figure 3-8: Welch periodogram and PSD of output data from the second area of the example model.	27
Figure 3-9: Estimates of the PSD for each of the output channels from the modified example model.	29
Figure 3-10: Estimate of the spectral coherence between the modified model’s first and third outputs. Note the lack of a peak near 0.5 Hz.	29
Figure 3-11: Spectral method mode shape estimates based on ambient data from the example model.	31
Figure 3-12: Ambient and transient data from the example model.	32
Figure 3-13: Response of the example system’s third output to a step change at input 3.	33
Figure 3-14: Response of the example system’s third output to an impulse at input 3.	33
Figure 3-15: Transient response term for $\sigma_m = -0.176$, which leads to a damping ratio of 7%. In regard to this mode, the system is stable.	34

Figure 3-16: Transient response term for $\sigma_m = 0.176$, which leads to a damping ratio of -7% and unstable system conditions.	34
Figure 3-17: Inputs to the example model and the resulting transient responses apparent in the model's outputs.	36
Figure 3-18: Portion of data from output 2 used for analysis (black).	37
Figure 3-19: Estimated contribution of the damped sinusoids associated with each mode in Table 3-3 to the transient in output 2.	38
Figure 3-20: The signal used for analysis (black) and the modeled signal based on the mode estimates (red) for output 2.	39
Figure 3-21: Estimated contribution of the damped sinusoids from the split mode listed in Table 3-5 to the transient in output 2.	40
Figure 4-1: Real-world example of a forced oscillation apparent in time-domain PMU data.	42
Figure 4-2: Fourier series coefficients of the 0.2 Hz square wave input to the example model's third area to induce a forced oscillation.	43
Figure 4-3: Frequency response of the example system from input 3 to output 2.	44
Figure 4-4: Fourier series coefficients for the forced oscillation portion of output 2.	44
Figure 4-5: Forced oscillation portion of the output from the test model's second area.	45
Figure 4-6: Welch periodogram of the output from the test model's second area. Peaks corresponding to forced oscillation frequencies are apparent at odd harmonics of the input oscillation's 0.2 Hz fundamental frequency.	46
Figure 4-7: Forced oscillation components of the example model outputs in response to a 0.2 Hz sinusoid injected at the model's second input.	48
Figure 4-8: Shape of a 0.2 Hz forced oscillation injected at the model's second input.	48
Figure 4-9: Forced oscillation components of the example model outputs in response to a 0.2 Hz sinusoid injected at the model's third input.	49
Figure 4-10: Shape of a 0.2 Hz forced oscillation injected at the model's third input.	50
Figure 4-11: Forced oscillation components of the example model outputs in response to a 0.4 Hz sinusoid injected at the model's third input.	50
Figure 4-12: Shape of a 0.4 Hz forced oscillation injected at the model's third input.	51
Figure 4-13: Four possible scenarios when attempting to detect forced oscillations.	52
Figure 4-14: Energy in each minute of measured data in Figure 4-1. A hypothetical detection threshold is indicated by the red line.	54
Figure 5-1: Demonstration of the similarity between a forced oscillation (30-60 seconds) and a sustained natural oscillation (90-120 seconds).	57
Figure 5-2: Measurements analyzed to monitor the system's electromechanical modes.	58
Figure 5-3: Welch periodogram of the first 10 minutes of ambient data in Figure 5-2.	58

Figure 5-4: Welch periodogram of the second 10 minutes of data in Figure 5-2..... 59

List of Tables

Table 2-1. List of base electromechanical modes in the model used to generate example data...	16
Table 3-1. List of continuous-time pole estimates from the application of the LS method to ambient data. Those corresponding to the model's electromechanical modes are bold and are followed by the true values in parenthesis.	23
Table 3-2. List of electromechanical modes in the modified model used to generate data for Example 3.	30
Table 3-3. Mode estimate results from application of Prony's method to modeled data. Estimates corresponding to true modes are listed in bold with true values in parenthesis.	37
Table 3-4. Mode shape estimates from application of Prony's method to modeled data. Estimates corresponding to true modes are listed in bold. All estimates have been normalized using output 2 as reference.	37
Table 3-5. Mode estimate results from application of Prony's method to modeled data with a high model order of 22. The "split mode" estimates are highlighted in bold font.	40
Table 5-1. Actual and estimated mode frequency and damping values for ambient data and data containing a forced oscillation.	59

1. Introduction

Oscillatory behavior in power systems has been and remains of great interest to engineers and researchers. In the past, most of this interest was placed on modal, i.e., natural, oscillations because of their relationship to system-wide events. Recently, a great deal of work has focused on forced oscillations, which can be related to equipment misoperation or failure. As interest in forced oscillations has increased, so has the need for a common understanding of oscillation sources, characteristics, analysis techniques, and associated terminology. A good first step towards such a common understanding was made by the Joint Synchronized Information Subcommittee (JSIS) of the Western Electricity Coordinating Council (WECC) with the development of a document providing brief definitions, descriptions, and examples related to power system oscillations (Trudnowski D. , Pierre, Donnelly, & Venkatasubramanian, 2015). The goal of the present document is to build from this foundation to provide a more comprehensive discussion.

A key goal of this document is to communicate the connections between an oscillation's source, its resulting characteristics, and how it can be properly analyzed. Common pitfalls and descriptions of why analysis techniques fail when applied to the wrong oscillation type will also be provided. Though a broad set of references for established methods is included, only a selection of algorithms will be used for examples due to the vastness of the power system oscillation analysis literature. This document does not make an effort to compare the performance of various algorithms, except where demonstrating that an algorithm is not designed for a specific application. Rather, examples using a specific algorithm are intended to represent the operation of a broader class of analysis techniques. Before beginning, a detailed discussion of power system oscillations and analysis techniques, some background and overviews for topics in the document are provided in the following section.

2. Background

A brief overview of the theory that will be referenced throughout the document is provided in this section. To begin, Section 2.1 provides an overview of the system responses that are the focus of this document. A description of how measurements containing these system responses are used to develop measurement-based models is provided in Section 2.2. Signal processing considerations important to the successful fitting of these models are described in Section 2.3. Finally, Section 2.4 contains a description of the simple model that has been used to generate the example data analyzed throughout this document. In this section, only enough information to provide context for the rest of the document has been provided, so the authors refer the interested reader to the referenced texts for more detailed discussions.

2.1. Overview of System Responses

Depending on initial conditions and inputs, systems can display a variety of responses in their measured outputs. The development of Phasor Measurement Unit (PMU) networks has dramatically increased the availability of measurements containing these system responses. Commonly observed and analyzed responses related to power system oscillations were defined in (Trudnowski D. , Pierre, Donnelly, & Venkatasubramanian, 2015). These definitions, with some additional clarifications for this document, are listed below. Examples of the various responses are provided in Figure 2-1.

Natural Response: A **Natural Response** is an oscillation characterized by the oscillatory modes only. In this document, inter-area electromechanical modes are considered specifically.

Ambient Response: An **Ambient Response** is the response of the system to the small random changes within the system. These changes are typically characterized by small random load changes. They are an example of a **Natural Response**.

Transient Response: A **Transient Response** is the response of the system immediately after a sudden disturbance, such as a fault, line tripping, generator trip, or load tripping. Small-scale transient responses are typically characterized by a **Natural Response**.

Forced Response: A **Forced Response** is the response of the system associated with an external input or a malfunctioning apparatus. Examples include a malfunctioning steam valve cycling on and off, or an arc furnace inducing its dynamics into the grid. **Forced oscillations** may include harmonics resulting from the periodicity of the external inputs.

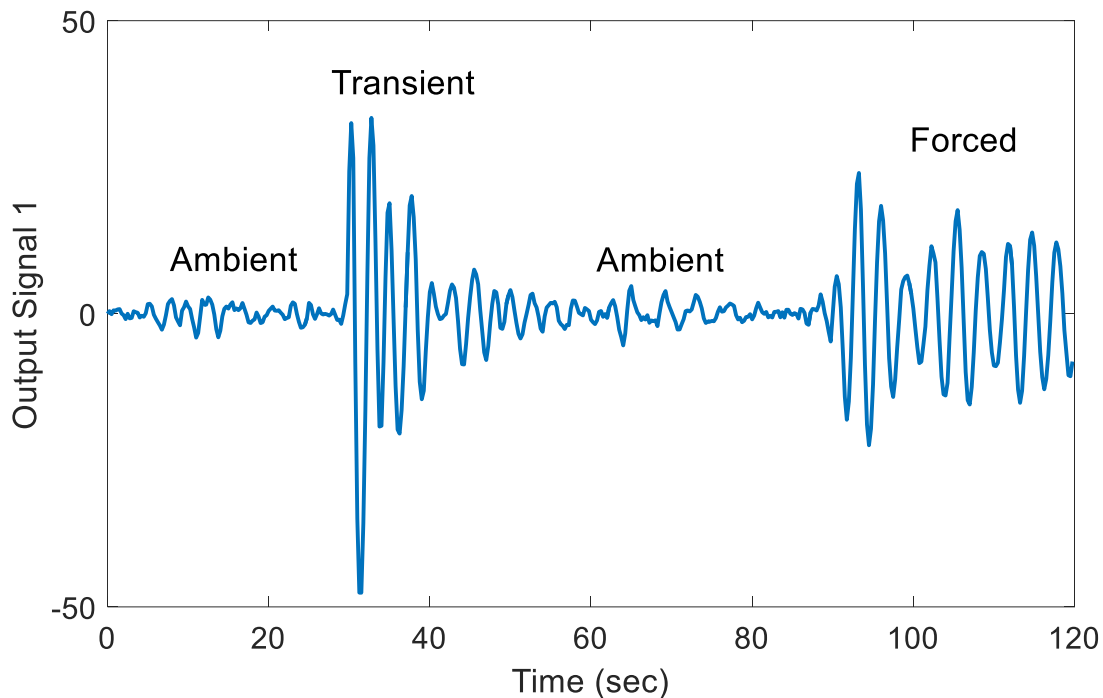


Figure 2-1: Typical examples of ambient, transient, and forced responses. The model used to generate this output is described in Section 2.4.

Natural responses, as indicated in the definition above, are related to the system's dynamics through the electromechanical modes of oscillation. In a power system, inter-area electromechanical modes are a characteristic of how generators in disparate parts of the system exchange energy. This exchange manifests as low-frequency oscillations (generally between 0.1 and 1 Hz) in electrical and mechanical power, as well as other related parameters. Along with frequency, the modes are often characterized by their damping and shape. A mode's damping influences how quickly (and if) a related oscillation subsides, and is therefore the parameter most closely tied to system stability. A mode's shape describes the grouping and relative participation of generators in an oscillation. It is parameterized by a magnitude and angle at each measurement

location. Generators in areas where the mode shape magnitude is largest are the strongest participants in the mode. Generators with similar mode shape angles tend to oscillate together. They oscillate against, i.e., exchange energy with, generators from areas where the mode shape angles are nearly 180° away. When natural response oscillations occur in power systems, their characteristics – frequency, damping, and shape – are inherited from the system’s modes.

In contrast, the form of a forced response depends on the input driving the oscillation. For example, the frequencies of forced oscillations are determined by the frequency of their associated input, regardless of the frequencies of the system’s inter-area electromechanical modes. The fundamental distinction between natural and forced responses can be summarized as follows: the form of a natural response depends on the system, while the form of a forced response depends on the driving input. This distinction explains why natural responses, but not forced responses, can be analyzed to estimate the system’s inter-area electromechanical modes.

Because the power system behaves linearly in the vicinity of a steady-state operating point, the outputs of the system are the superposition of the various responses. For example, when a forced oscillation is occurring in otherwise ambient conditions, the outputs of the system are sums of natural and forced responses. In some cases, which will be described in this document, it is important to consider the presence of the forced response in order to properly analyze the natural response. If the forced response is not considered, measurement-based models, such as those described in the following section, may poorly reflect the true system.

2.2. Overview of Measurement-Based System Models

One approach to estimating a power system’s electromechanical modes is to build a detailed model of the system and its components. This document focuses on a complementary approach that uses power system measurements to create models of the system and associated signals. These system models do not include generators, transmission lines, etc. Instead, they are mathematical descriptions of how the power system translates inputs to measured outputs. Measurements from PMU networks are particularly useful for this task because they are synchronized and geographically dispersed.

By analyzing measurements, which contain the system responses described in the previous section, specific values for the model’s parameters can be selected. Once this is done, the relationship between the model’s structure and the system’s electromechanical modes can be exploited to estimate the modes. To provide examples of these relationships and for reference throughout the document, the following subsections provide overviews of two models that are commonly used in measurement-based modal analysis.

2.2.1. State-Space Models

In this section, a brief discussion of state-space models is provided. A fuller treatment of this material can be found in (Kundur, 1994). State-space models represent the system using a set of ordinary differential equations of the form

$$\dot{\underline{x}}(t) = A\underline{x}(t) + B_e\underline{e}(t) + B_u\underline{u}(t) \quad (1a)$$

$$\underline{y}(t) = C\underline{x}(t) + D\underline{e}(t) + \underline{\mu}(t) \quad (1b)$$

where $\underline{x}(t)$ is the state vector, $\underline{e}(t)$ is a vector of random system perturbations, $\underline{u}(t)$ is a vector that describes control actions such as low-level probing and load pulses, $\underline{\mu}(t)$ is measurement noise, $\underline{y}(t)$ is the measured output of the system, and t is time. A closer examination of this model, particularly the input vectors $\underline{e}(t)$ and $\underline{u}(t)$ will be provided in later sections. Here, the relationship between the state matrix A and the system's inter-area electromechanical modes will be examined.

The eigenvalues of the state matrix are the complex valued λ_i that satisfy the characteristic equation given by

$$\det(A - \lambda I) = \lambda^{n_a} + a_1\lambda^{n_a-1} + \dots + a_{n_a-1}\lambda + a_{n_a} = 0 \quad (2)$$

where n_a is the order of the square matrix A , I is an appropriately sized identity matrix, and $i = 1, 2, \dots, n_a$. These eigenvalues are complex valued and are often expressed as

$$\lambda_i = \sigma_i + j\omega_i. \quad (3)$$

A subset of these eigenvalues correspond to the system's dominant inter-area electromechanical modes. To identify which ones, the frequencies

$$f_i = \frac{\text{Imag}(\lambda_i)}{2\pi} \quad (4)$$

with units of Hz, damping ratios

$$\zeta_i = -\frac{\sigma_i}{|\lambda_i|} \times 100 = -\cos(\angle\lambda_i) \times 100 \quad (5)$$

with units of percent, and associated mode shapes can be examined. Because complex eigenvalues appear in conjugate pairs, it is common to focus on those with positive frequencies.

Letting \underline{v}_i denote the right eigenvector corresponding to eigenvalue λ_i , the mode shape between states p and l is expressed as a magnitude

$$|MS_{pl}| = \frac{|v_{i,p}|}{|v_{i,l}|} \quad (6)$$

along with angle

$$\angle MS_{pl} = \angle v_{i,p} - \angle v_{i,l} \quad (7)$$

where $v_{i,p}$ denotes the p^{th} element of the i^{th} eigenvector. Mode shape is normally evaluated by comparing states from throughout the system with a reference state. The mode shape magnitudes relate the level of participation of states in an oscillation, while the angles indicate which states are grouped together in the oscillation.

Often, the mode shape between measured system outputs is desired if the system states are not directly measured, e.g., using substation voltage angle from a PMU rather than a generator rotor angle. The mode shape between measured outputs relates to that of the system states by first pre-multiplying the right eigenvectors by output matrix C , i.e., $\underline{v}_i^{(y)} = C\underline{v}_i$. The mode shape between measured outputs 1 and 2 thus become

$$\left| MS_{12}^{(y)} \right| = \frac{\left| v_{i,1}^{(y)} \right|}{\left| v_{i,2}^{(y)} \right|} \quad (8)$$

and

$$\angle MS_{12}^{(y)} = \angle v_{i,1}^{(y)} - \angle v_{i,2}^{(y)} \quad (9)$$

Because measurement-based modal analyses are based on sampled data, the relationship between the continuous-time model described thus far and the discrete-time state-space model

$$\underline{x}(k+1) = A^D \underline{x}(k) + B_e^D \underline{e}(k) + B_u^D \underline{u}(k) \quad (10a)$$

$$\underline{y}(k) = C \underline{x}(k) + D \underline{e}(k) + \underline{\mu}(k) \quad (10b)$$

is important to consider. Here k is the sample index corresponding to time $t = kT$ where T is the sampling interval,

$$A^D = e^{AT} \quad (11)$$

is the discrete-time version of the state-matrix in (1a), and B_e^D and B_u^D are the discrete-time versions of the input matrices in (1a) (Kamen & Heck, 2007). There is no difference between the continuous- and discrete-time versions of C and D (Kamen & Heck, 2007). The eigenvalues of A^D are the complex valued z_i satisfying

$$\det(A^D - zI) = z^{n_a} + a_1 z^{n_a-1} + \dots + a_{n_a-1} z + a_{n_a} = 0. \quad (12)$$

They are related to the continuous-time eigenvalues through

$$\lambda_i = \frac{1}{T} \ln(z_i). \quad (13)$$

Because the continuous-time eigenvalues appear in conjugate pairs, the discrete-time eigenvalues do as well. Measurement-based modal analysis methods based on a state-space model estimate the matrices in (10) and then use the relationships described in this section to obtain estimates of the electromechanical modes as continuous-time eigenvalues. The mode shape estimates are obtained directly from the eigenvectors of A^D as with the continuous-time case.

2.2.2. ARMAX Models

Though AutoRegressive Moving Average eXogenous (ARMAX) models can model inputs and outputs as vectors, in power system applications they are often implemented with scalar inputs and outputs. In this document, this simplified case is considered. The ARMAX model can then be expressed as the difference equation

$$y(k) = -\sum_{i=1}^{n_a} a_i y(k-i) + \sum_{i=0}^{n_b} b_i u(k-i) + \sum_{i=1}^{n_c} c_i e(k-i) + e(k) \quad (14)$$

where k is the sample index corresponding to time $t = kT$ with sampling interval T , $y(k)$ is the measured system output, $u(k)$ is a deterministic input, $e(k)$ models aggregated random system perturbations, n_a is the AR model order, n_b is the X model order, and n_c is the MA model order. For $u(k) = 0$, the transfer function obtained by applying the z-transform to (14) is

$$\frac{Y(z)}{E(z)} = \frac{1 + \sum_{i=1}^{n_c} c_i z^{-i}}{1 + \sum_{i=1}^{n_a} a_i z^{-i}} = \frac{z^{n_a} (1 + \sum_{i=1}^{n_c} c_i z^{-i})}{z^{n_a + a_1} z^{n_a - 1} + \dots + a_{n_a - 1} z + a_{n_a}}. \quad (15)$$

Note the relationship between the roots of the denominator polynomial, which as the model's poles determine its stability, and (12). Mode-estimation algorithms operate by estimating the coefficients in (14), finding the roots of the denominator polynomial in (1), and converting to continuous-time poles via (13). The frequency and damping ratio of electromechanical modes can then be obtained using (4) and (5). Note that mode shape cannot be evaluated with a model based on measurements from a single location. Multi-channel ARMAX methods do exist that can estimate mode shape along with the modes (Dosiek & Pierre, Estimating electromechanical modes and mode shapes using the multichannel ARMAX model, 2013), but because most of the concepts in this paper can be discussed with a single-input single-output model, this simpler approach is taken.

2.3. Signal Processing Considerations

The proper application of signal processing techniques to power system measurements is crucial when fitting the models described in the previous section. It can also make the distinguishing characteristics of oscillatory behaviors more apparent. In this section, the discussion focuses on three of the most important aspects of a signal that warrant consideration: record length, sampling rate, and frequency. A brief description of these aspects and how they can be manipulated is provided here as background to discuss proper analysis techniques later in the document.

Generally, signal processing algorithms perform better as the record length increases for a fixed sampling rate. This is of particular interest in power system applications due to their challenging nature. However, power systems are constantly changing, so it is often important to limit record

lengths to capture a single operating condition. For example, algorithms used to monitor the electromechanical modes in near-real time would be useless if applied to multiple hours of data because the modes can change dramatically within that time span. To obtain accurate and informative estimates, it is important that the user selects an appropriate record length. Similarly, the sampling rate is an important consideration.

The fundamental importance of the sampling rate of a signal is that it limits the range of the signal's frequency content that can be reliably observed. For the common PMU frame rates of 30 and 60 frames per second, frequencies up to 15 and 30 Hz, respectively, can be observed. For some applications, particularly analysis of electromechanical modes, it is beneficial to limit the frequency range to more narrowly cover the range of interest. This is accomplished by decimation, which is the process of lowering the sampling rate of a signal by removing samples after applying an appropriate filter. For example, decimating to 5 samples per second limits the observable frequency range from 0 to 2.5 Hz.

For a visual, though not rigorous, explanation of how adjusting a signal's frequency content can impact analysis, recall that the electromechanical modes are captured in the models as the discrete-time poles z_i . From (13), the discrete-time poles can be written in terms of their continuous-time counterparts as

$$z_i = e^{T\lambda_i} = e^{T(\sigma_i + j\omega_i)} = e^{T\sigma_i} e^{jT\omega_i} = e^{T\sigma_i} \angle T\omega_i = e^{T\sigma_i} \angle 2\pi \frac{f_i}{f_s}, \quad (16)$$

where f_i is the frequency of the i^{th} mode in units of Hz and f_s is the sampling rate of the signal. As an aside, note that the z_i will remain inside the unit circle as long as $\sigma_i < 0$, which relates well known conditions for stability in discrete- and continuous-time systems. With (16) in mind, consider a system's dominant electromechanical modes, which tend to have frequencies between 0.1 and 1 Hz and damping ratios (well) below 20%. For a high sampling rate of $f_s = 60$, the z_i for these frequencies and damping ratios will be in the range indicated in Figure 2-2. It is difficult for algorithms to accurately estimate multiple modes in such a small region. However, after decimating to $f_s = 5$, the z_i will be in the much larger region depicted in Figure 2-3. Signal processing algorithms tend to be better able to estimate multiple modes in this larger region. To understand why, note that for any value of λ_i in (16), the z_i approach $(1 \angle 0^\circ)$ as f_s increases and, consequently, T decreases. This behavior tends to introduce numerical problems. Further, high sampling rates force algorithms to fit models to high frequency noise well beyond the true system bandwidth. For further discussion, see (Ljung, 1999).

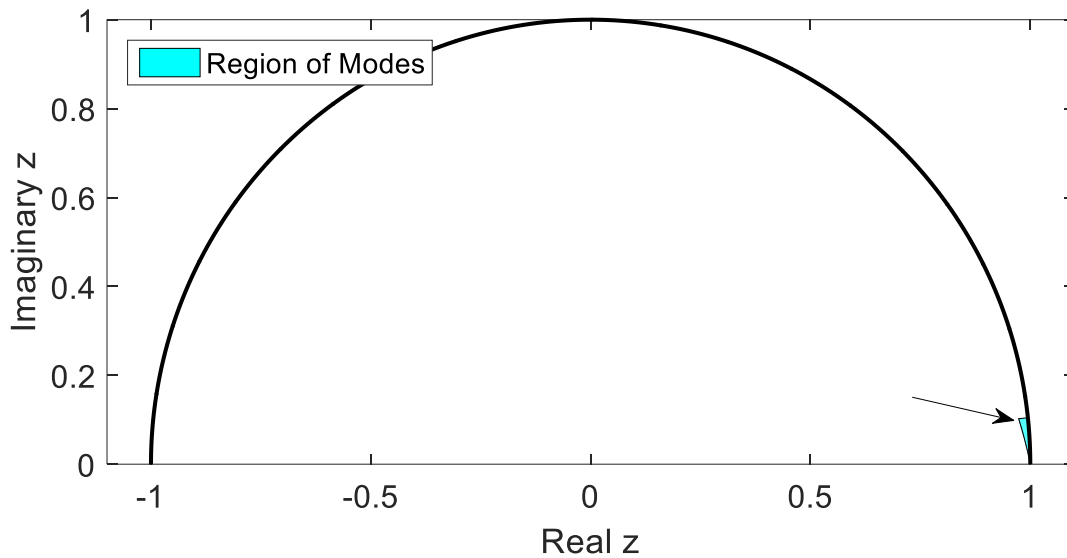


Figure 2-2: Region in the z-domain that electromechanical modes tend to occupy for a sampling rate of 60 samples per second.

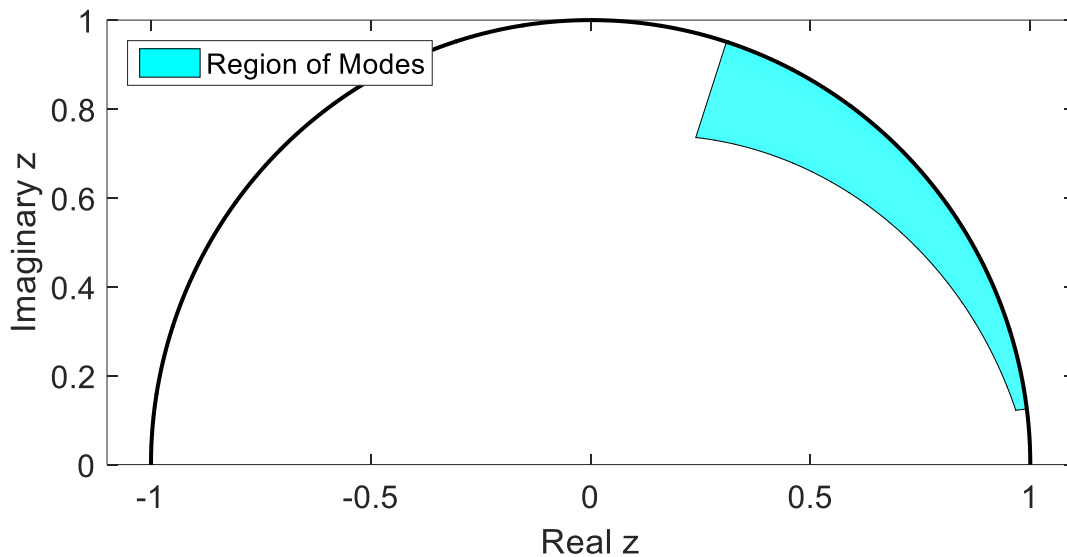


Figure 2-3: Region in the z-domain that electromechanical modes tend to occupy for a reduced sampling rate of 5 samples per second.

As mentioned previously, decimating is accomplished by filtering the signal and then removing samples to lower the sampling rate. Without filtering, the frequency content and sampling rate of the signal would not match, leading to aliasing. Anti-aliasing filters are only one variety of filters that are useful in the analysis of power system oscillations.

Filtering can be implemented for a variety of reasons, but its general purpose is to limit the frequency content of a signal to improve analysis results. For example, it may be beneficial to remove the low-frequency trends of a signal via high-pass filtering to eliminate the effects of

generators ramping up and down or to remove DC components. Properly filtering a signal can improve the signal processing results, but it must be done with care to avoid distorting signals in undesirable ways. The same is true with all of signal processing – care must be taken. For each of the oscillation behaviors described in the following sections, some comments and cautions regarding proper signal processing are provided.

2.4. Simple Model for Example Data Generation

Previous subsections have focused on theory that will be referenced throughout the document. In this section, the simple model used to generate data for examples throughout this report is described. The model is based on transfer functions, which are one approach to describing how a set of inputs to a system are manipulated to form a set of outputs. A conceptualization of the model is presented in Figure 2-4. Each input and output corresponds to one of three areas. The areas are connected, so every input affects every output. To describe these interactions, transfer functions to the three outputs were designed for each input, resulting in a total of nine transfer functions. Each was designed with an identical denominator to model the inter-area electromechanical modes with base characteristics listed in Table 2-1. Residues were assigned to each mode for each input-output pair to achieve the shapes listed in Table 2-1. As a result, the numerators for each transfer function are unique.

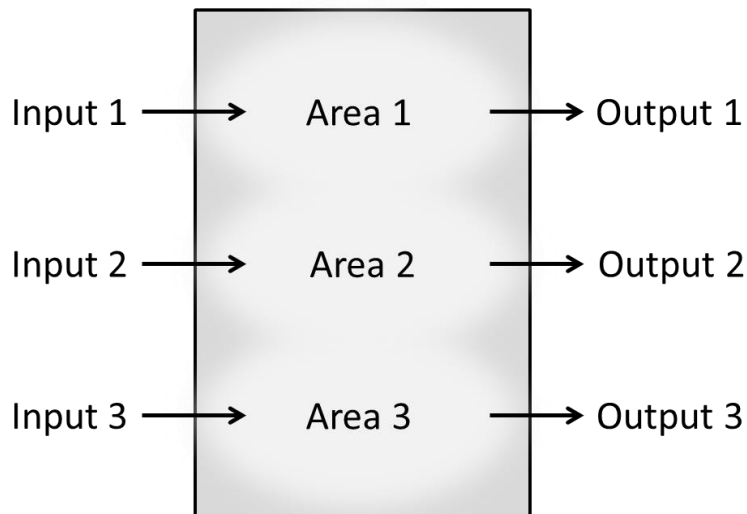


Figure 2-4: Conceptualization of the simple transfer function model used to generate example data.

Table 2-1. List of base electromechanical modes in the model used to generate example data.

Frequency (Hz)	Damping Ratio (%)	Shape	
		Group 1	Group 2
0.25	7	Areas 1 & 3	Area 2
0.4	7	Area 1	Area 2
0.6	6	Area 2	Area 3

The model was developed to generate signals that exhibit characteristics observed in power system measurements, rather than to properly model the individual components of a power system or specific real-world events. Inputs to the system were designed to elicit specific oscillation behaviors in the outputs. These inputs will be described in later sections for each of the oscillation behaviors that are the focus of this document.

3. Natural Response Oscillations

In this section, oscillations related to the natural responses of power systems will be described. Their sources, related characteristics, and proper analysis techniques will be discussed. As described in Section 2.1, natural response oscillations are those with forms determined by the system itself, though ambient- and transient-type natural oscillations are quite distinct in appearance. Due to their differences, their characteristics and proper analysis techniques also differ. Thus, they will be described separately in Sections 3.1 and 3.2.

3.1. Ambient Response

The ambient response of a power system can be useful for continuous near-real time monitoring or off-line benchmarking of the system's inter-area electromechanical modes. A variety of analysis techniques have been developed to accomplish this task. In the following sections, the sources, characteristics, and analysis techniques for ambient responses will be discussed.

3.1.1. Sources of Ambient Responses

Recall from Section 2.1 that an ambient response is the response of the power system to the small random changes within the system. These small changes may include system load, varying generation effects, system switching effects, and small disturbances (Pierre, Trudnowski, & Donnelly, 1997). Over the span of several minutes, the primary component of the ambient noise is driven by random load changes. These random changes act as a constant excitation to the electromechanical dynamics of the power system. As a result, they effect the voltage, current, power, and frequency measurements produced by PMUs.

As an example, consider the response of the transfer-function model in Figure 2-4 of Section 2.4 to white noise inputs. The white noise at each of the system's inputs represents random load changes in the system. The top plot in Figure 3-1 is the white noise injected in Area 1, while the bottom plot is the ambient noise response from the same area. Note that this response, which is the combination of responses from each input, has a significantly different appearance in the time domain because it was colored by the model's dynamics. Still, the system response is not obviously oscillatory; it is very noisy in appearance. This, and other characteristics, will be discussed in the following section.

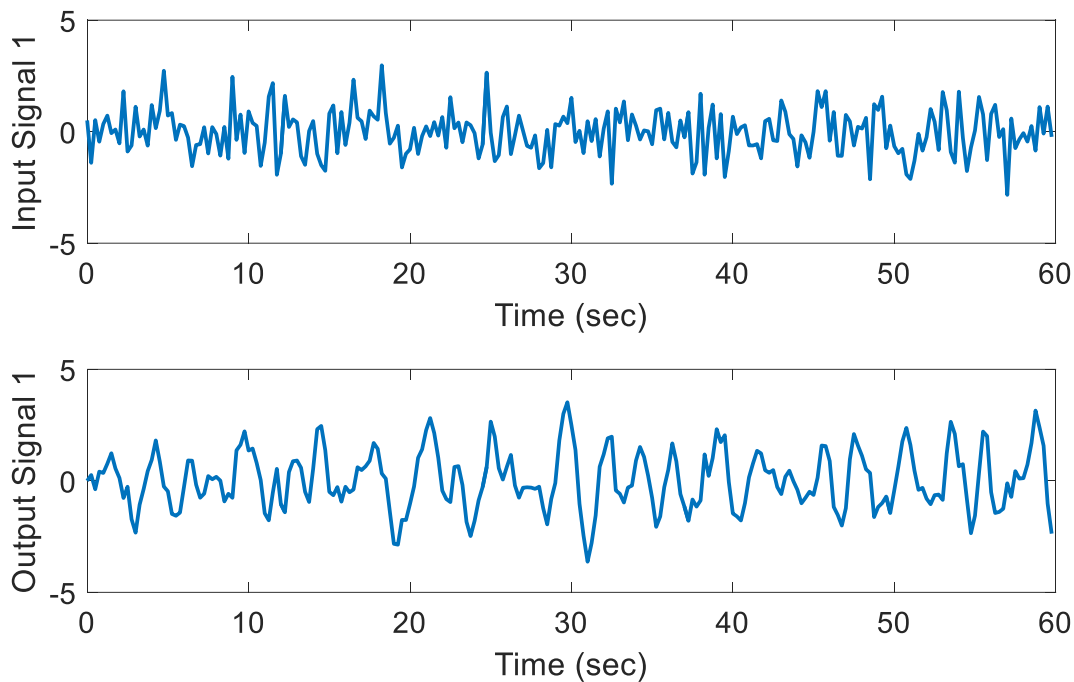


Figure 3-1: Example white noise input (top) to the example system and resulting ambient noise response from the system (bottom).

3.1.2. Characteristics of Ambient Responses

Though the output signal in Figure 3-1 is quite different from the input signal, it is not obvious how the system's characteristics are reflected in the response or how the signal constitutes an oscillation. Unlike a ringdown, the ambient response is a random process. As such, each set of ambient noise appears quite unique in the time domain. However, examination in the frequency domain provides a wealth of insight.

The power spectral density (PSD) of the example model's second output is displayed in Figure 3-2. The PSD describes how a signal's power is distributed over frequency. Here, the PSD is available because a model is being used. For power system measurements, the PSD can be estimated from ambient data using a variety of approaches. Note that the peaks in the PSD correspond to the example model's electromechanical modes. Their frequencies and damping ratios are listed in the figure. By centralizing the ambient noise's frequency content around the frequencies of the electromechanical modes, the system dictates the form of the natural ambient response.

Under different system conditions, the characteristics of the ambient noise also change. For example, consider Figure 3-3, which displays the PSD of the model's second output after the frequency and damping ratio of each of the model's electromechanical modes was modified. Similar changes in the electromechanical modes of real power systems take place when system modifications, such as generation redispatch or topology changes occur. Note that the peak locations have shifted to the new modal frequencies. The height of each peak is also affected by the damping ratios of the modes, with lower damping ratios corresponding to higher peaks. With the change in frequency content introduced by an adjustment to the system's modes, the ambient

noise will likewise change. Again it can be emphasized that the system's natural response takes a form associated with the system itself. This characteristic allows the system's electromechanical modes to be estimated using ambient data.

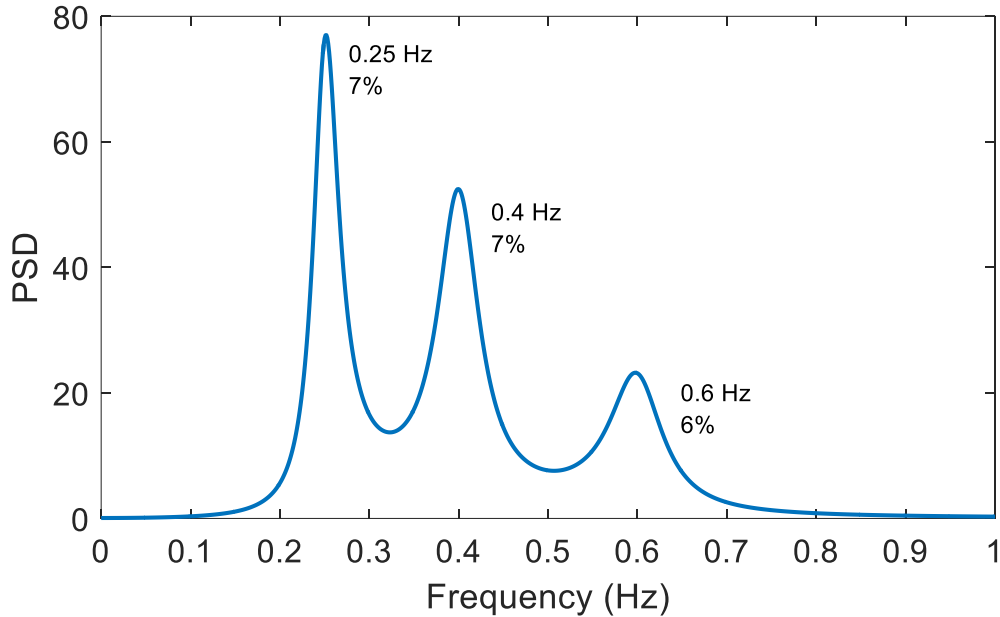


Figure 3-2: PSD of the example model's output signal from Area 2 in the base case. The frequency and damping ratio of each of the model's electromechanical modes are listed next to their associated peaks.

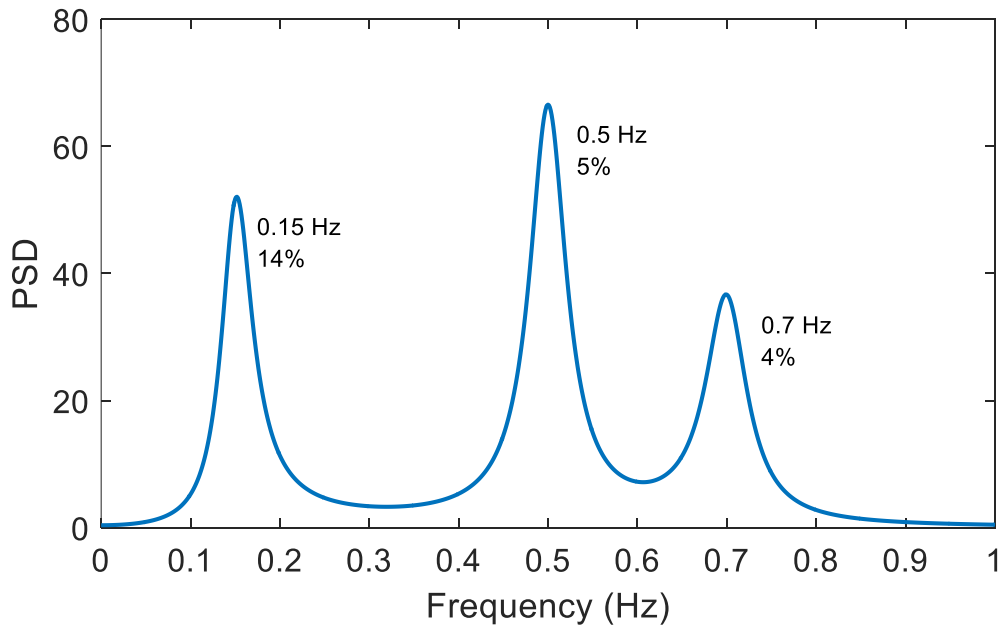


Figure 3-3: PSD of the example model's output signal from Area 2 with changes to the electromechanical modes. The frequency and damping ratio of each of the model's modes are listed next to their associated peak.

Before discussing analysis techniques, it should be emphasized that analyses can be successfully conducted in either the time or frequency domains. It should not be assumed that frequency-domain approaches are superior because the modes are apparent in the PSD, which again, is a theoretical value that must be estimated in practice. Rather, the time- and frequency-domain signals are closely coupled, allowing for analysis in either domain. In the following section, both varieties of analysis are considered.

3.1.3. Analysis of Ambient Responses

As discussed previously, random load changes that constantly excite the electromechanical dynamics of the power system result in a natural system response of colored ambient noise that is captured in PMU measurements. As a result, the ambient noise can be analyzed to estimate the electromechanical modes. There are a variety of methods available to do so, and they include time-domain, frequency-domain, and subspace approaches. Though useful tools, subspace methods will not be discussed in this document due to their complexities. The interested reader is directed to (Kamwa & Gerin-lajoie, 2000), (Zhou, Pierre, & Wies, 2003), (Ghasemi, Canizares, & Moshref, 2006), and (Jingmin, Chen, & Feng, 2011) for information on these methods.

3.1.3.1. Time-Domain Methods

Some of the most common time-domain approaches are related to the ARMAX model, which was discussed in Section 2.2.2. Repeated from (14), the difference equation describing the model is

$$y(k) = -\sum_{i=1}^{n_a} a_i y(k-i) + \sum_{i=0}^{n_b} b_i u(k-i) + \sum_{i=1}^{n_c} c_i e(k-i) + e(k).$$

Some classic approaches to estimating the coefficients of this equation, or its simplifications, are the least-squares (LS), Yule-Walker (YW), and maximum likelihood methods (Ljung, 1999). Each of these approaches is based on characteristics of the measured signal, $y(k)$, that can be represented with this model. For example, the YW method relies on the autocovariance sequence of $y(k)$, which is defined as

$$r(g) = E\{y(k)y(k-g)\}, \quad (17)$$

where $E\{\cdot\}$ denotes the expectation operator. From (14) and (17), it can be shown that the autocovariance sequence can be written in terms of the AR coefficients as

$$r(g) + \sum_{i=1}^{n_a} a_i r(g-i) = 0, \quad \text{for } g > n_c \quad (18)$$

when the deterministic input $u(k) \equiv 0$. This equation leads to an approach for estimating the AR coefficients, which can then be used to estimate the electromechanical modes, as discussed in Section 2.2.2. Here, the details of the YW algorithm are less significant than the general point that the ARMAX model captures characteristics of ambient power system data that can be used to estimate the electromechanical modes. This is demonstrated in more detail in the following example.

Example 1: Least-Squares Estimation of the Electromechanical Modes using Ambient Data

In this example, the electromechanical modes of the transfer-function model described in Section 2.4 will be estimated by applying the LS algorithm to ambient data generated by the model. Instead of the full ARMAX described by (14), the simplified AR model described by the difference equation

$$y(k) = -\sum_{i=1}^{n_a} a_i y(k-i) + e(k) \quad (19)$$

will be used. Note that due to the lack of a deterministic input, the exogenous (X) portion of the ARMAX model is unnecessary, and by using a sufficiently high model order, the AR model can be used in place of the full ARMA model.

For $k = n_a, n_a + 1, \dots, K$, (19) can be written in matrix form as

$$\begin{bmatrix} y(n_a + 1) \\ y(2) \\ \vdots \\ y(K) \end{bmatrix} = \begin{bmatrix} y(n_a) & y(n_a - 1) & \cdots & y(1) \\ y(n_a + 1) & y(n_a) & \cdots & y(2) \\ \vdots & \vdots & \cdots & \vdots \\ y(K - 1) & y(K - 2) & \cdots & y(K - n_a) \end{bmatrix} \begin{bmatrix} a_1 \\ a_2 \\ \vdots \\ a_{n_a} \end{bmatrix} + \begin{bmatrix} e(n_a + 1) \\ e(2) \\ \vdots \\ e(K) \end{bmatrix} \quad (20)$$

or in compact notation as

$$\underline{y} = Y\underline{\theta} + \underline{e}. \quad (21)$$

Note that $Y\bar{\theta}$ should closely match \underline{y} . Thus, the estimate of $\underline{\theta}$, denoted here as $\hat{\underline{\theta}}$, should be selected to minimize $\underline{y} - Y\hat{\underline{\theta}}$. Noting that Y is not square and denoting the matrix transpose with a superscript T , this is accomplished by the LS estimate

$$\hat{\underline{\theta}} = -(Y^T Y)^{-1} Y^T \underline{y}. \quad (22)$$

Though this is an incomplete derivation, it does show how electromechanical mode estimates can flow directly from the ARMAX difference equation.

Applying (22) to 10 minutes of data from output channel 2 of the example model with $n_a = 16$ leads to the coefficient estimates

$$\underline{\hat{\theta}} = \begin{bmatrix} \hat{a}_1 \\ \hat{a}_2 \\ \vdots \\ \hat{a}_{16} \end{bmatrix} = \begin{bmatrix} -1.1028 \\ 0.6040 \\ 0.2504 \\ 0.0502 \\ 0.0673 \\ 0.1330 \\ 0.1372 \\ 0.1585 \\ 0.1506 \\ 0.0640 \\ 0.0830 \\ 0.1374 \\ 0.0182 \\ 0.1147 \\ 0.0353 \\ 0.0724 \end{bmatrix}.$$

Portions of the measured input data \underline{y} and the reconstructed signal $Y\hat{\underline{\theta}}$ using the estimates above are plotted in Figure 3-4. The similarity between the signals indicates a good estimation result.

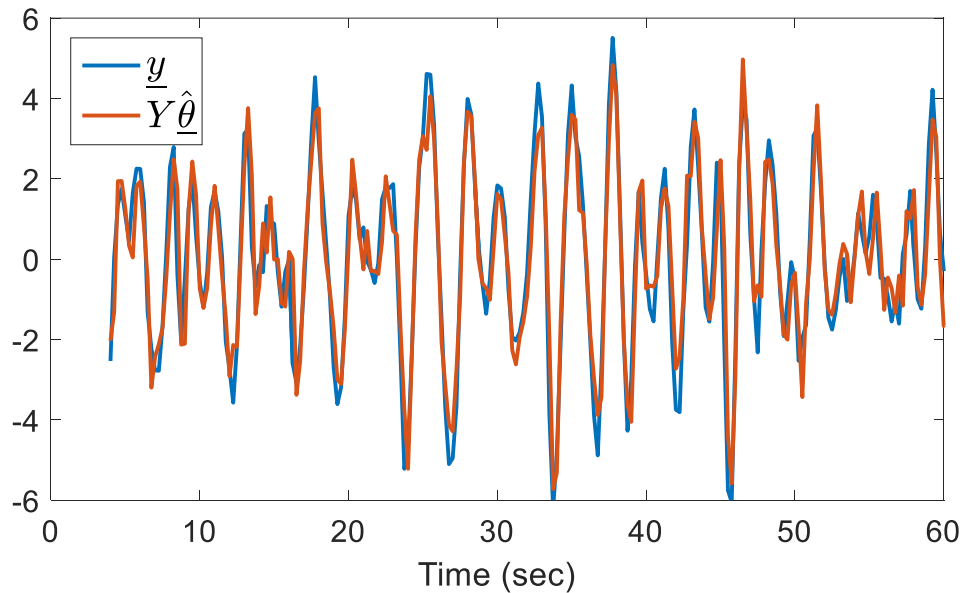


Figure 3-4: Input signal \underline{y} and reconstructed signal $Y\hat{\underline{\theta}}$ from the LS method.

Recall that the coefficients estimated above correspond to the polynomial in the denominator of the transfer function (1) that models the system. Thus, the roots of the polynomial correspond to the poles of the system, which dictate the system's stability. Rooting this polynomial to obtain the discrete-domain poles, transforming to continuous-time poles via (13), and calculating frequencies and damping ratios as in (4) and (5) leads

to the candidates for electromechanical mode estimates listed in Table 3-1. The entries listed in bold correspond to the model’s electromechanical modes, and the true values are listed in parenthesis. The other pole estimates result from using a model order in excess of the true system order to account for noise.

Table 3-1. List of continuous-time pole estimates from the application of the LS method to ambient data. Those corresponding to the model’s electromechanical modes are bold and are followed by the true values in parenthesis.

Frequency (Hz)	Damping Ratio (%)	Pseudo Energy (normalized)
0.245 (0.25)	6.65 (7)	1.00
0.401 (0.4)	7.66 (7)	0.96
1.326	16.08	0.13
<i>0.604 (0.6)</i>	<i>6.10 (6)</i>	<i>0.11</i>
0.812	16.37	0.05
1.103	13.08	0.05
1.559	8.69	0.02
1.855	6.42	0.01

Distinguishing between pole estimates that correspond to true modes from those that correspond to “noise modes” can be challenging. Note that the estimate with frequency 0.604 Hz is relatively close to the true system mode with frequency 0.6 Hz and damping ratio 6%. The pseudo energy is one tool that is useful in making the distinction. The pseudo energy is a measure of a mode’s observability in a set of measurements. Details on its calculation from ambient data can be found in (Trudnowski D. J., Pierre, Zhou, Hauer, & Parashar, 2008). Because the pseudo energy associated with the 0.604 Hz estimate is in the range of the noise modes, it is not listed as a reliable estimate of the true mode. Distinguishing between system and noise modes can also be guided by *a priori* information about the system, particularly mode frequency, damping, and shape.

This example demonstrated the use of the LS method to estimate the electromechanical modes of a system from ambient data. The AR(MA) model describing how random load changes result in colored ambient noise measured by PMUs led to the result. The key is that ambient noise, as a natural response of the system, takes a form dictated by the dynamics of the system and can therefore be analyzed to reveal information about those dynamics, namely, the electromechanical modes.

■

Mode Shape Estimation

Along with frequency and damping, mode shape can also be estimated by applying time-domain approaches to ambient data. Recall from Section 2.2.1 that the mode shape corresponding to electromechanical mode (eigenvalue) λ_i with right eigenvector v_i is given by evaluating the magnitude and angle of

$$MS_{pR} = \frac{v_{i,p}}{v_{i,R}}. \quad (23)$$

Mode shape is evaluated for several states p referenced to state R . As derived in (Zhou, Huang, Dosiek, Trudnowski, & Pierre, 2009),

$$G_{pR}(\lambda_i) = \frac{v_{i,p}}{v_{i,R}} \quad (24)$$

where $G_{pR}(\lambda_i)$ is the transfer function from state R to state p . Based on this relationship, the paper proposes a general mode shape estimation approach known as the transfer function method. To demonstrate this general approach, the paper applies the LS algorithm to identify the necessary transfer functions. The Channel Matching Method proposed in (Dosiek L. , Pierre, Trudnowski, & Zhou, 2009) is another parametric method for estimating mode shape via transfer functions. The method was shown to be a special case of the transfer function method in (Dosiek, Zhou, Pierre, Huang, & Trudnowski, 2013). Non-parametric methods that operate in the frequency domain will be discussed in the following section.

3.1.3.2. Frequency-Domain Methods

So far, the described analysis techniques have operated in the time domain. As discussed in Section 3.1.2, characteristics of ambient data related to a system's electromechanical modes can be observed in the frequency domain, making analysis methods based in this domain useful as well.

Spectral Estimation

One of the most straightforward approaches to analyzing data in the frequency domain is to estimate the PSD. Recall from Section 3.1.2 that the PSD is a theoretical value that quantifies how a signal's power is distributed over its frequency band. Ambient power system measurements tend to have significant content near the frequencies of the electromechanical modes that are observable at that point in the system. For example, all three modes are apparent in Figure 3-2 because the model's second area participates in all three modes (see Table 2-1). In Figure 3-5, however, the PSD of the example model's output from the first area barely contains a trace of the 0.6 Hz mode. Recall from Table 2-1 that the 0.6 Hz mode primarily dictates an oscillation between areas two and three in the model. The observability of a mode at various points in a power system is an important consideration. The shape of the PSD also indicates the level of each mode's damping, though it would be difficult to quantify the damping ratio by visual examination of the spectrum. Instead, the observation that spectral peaks narrow as the damping of the associated mode decreases provides a subjective measure of a mode's stability. Clearly, examination of the PSD can provide a wealth of information, but in power systems this theoretical value is not available, so it must be estimated.

Not all uses of spectral estimates are so subjective. For example, a method of estimating a mode's damping directly from a spectral estimate can be found in (Vanfretti, Bengtsson, Peric, & Gjerde, 2012). In (Liu & Venkatasubramanian, 2008), the authors describe how the singular value decomposition (SVD) can be applied to spectral estimates as part of an algorithm to estimate modal frequency, damping, and shape. Both of these approaches rely on nonparametric spectral estimation methods.

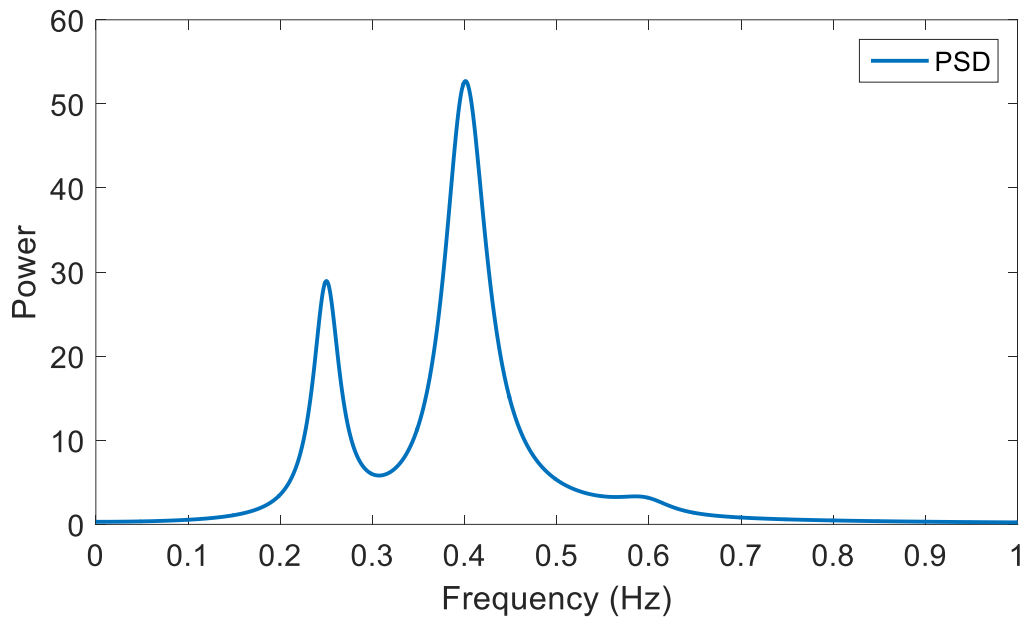


Figure 3-5: PSD of the example model’s output signal from Area 1 in the base case. Note that the 0.6 Hz mode is barely observable. See Table 2-1.

There are two broad categories of spectral estimators: parametric and nonparametric. Parametric estimators rely on fitting a model based on measured data, while nonparametric methods estimate the PSD directly from the data without using a model. Both of the models discussed in this document, the ARMAX and state-space models, can be used for parametric spectral estimation. For example, the spectral estimate in Figure 3-6 was generated using the LS estimates obtained in Example 1. Further details are not provided here, but the fundamental concept is that by modeling the way that inputs combine to form an output, models are also able to capture how the frequency content of each input is manipulated to dictate the frequency content of an output.

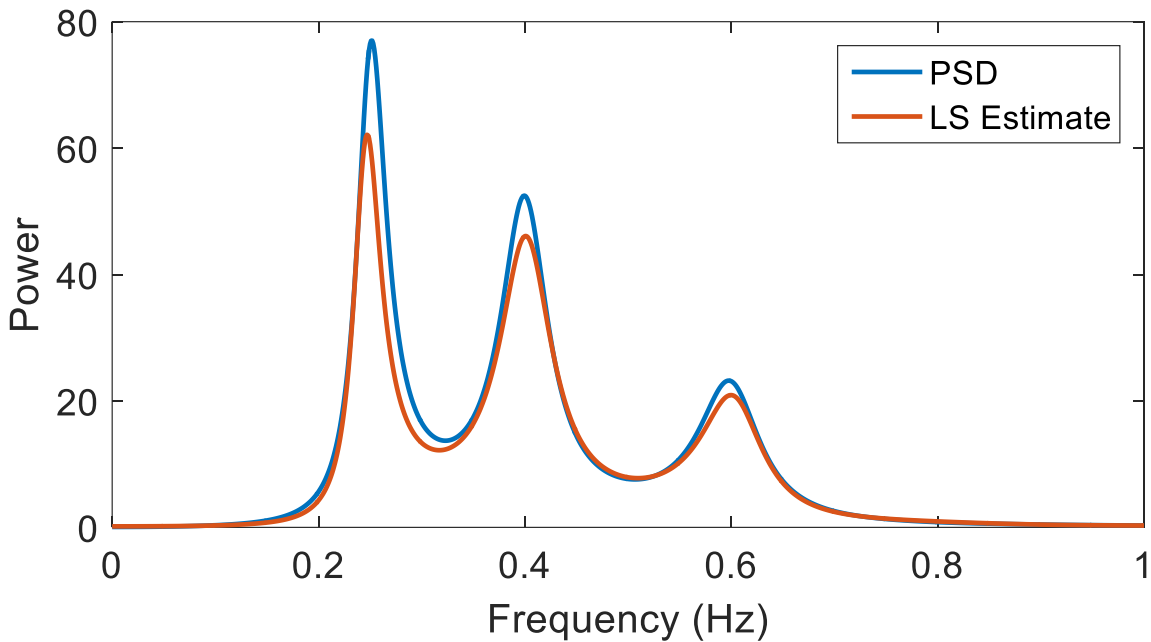


Figure 3-6: PSD and least-squares spectral estimate for measurements from the example model's second area.

Nonparametric methods rely on transforming time domain signals into the frequency domain, often using the discrete Fourier transform (DFT). Generally, outputs of the DFT are complex and correspond to a frequency bin between zero and half of the time-domain signal's sampling rate. Perhaps the simplest spectral estimator is the periodogram, which is simply

$$\hat{\phi}(f) = \frac{1}{K} |DFT\{y(k)\}|^2 \quad (25)$$

where f is a frequency variable and K is the signal length. The periodogram is a poor spectral estimator due to its variance, but this variance can be reduced using a variety of refined methods. One of the most common refined estimators, the Welch periodogram, is considered in the following example.

Example 2: Nonparametric Spectral Estimation of Ambient Data

The 10 minutes of Area 2 data from Example 1 is considered again in this example. To begin, the periodogram is obtained using a computationally efficient method of calculating the DFT. Any such method is known as a fast Fourier transform (FFT). Note that the FFT of the data is complex and cannot be considered an estimator of the PSD, though it is often misidentified as such. The periodogram of the data, calculated as in (25), is displayed in Figure 3-7 along with the PSD. Note that the estimate has significant variance, despite the long record length.

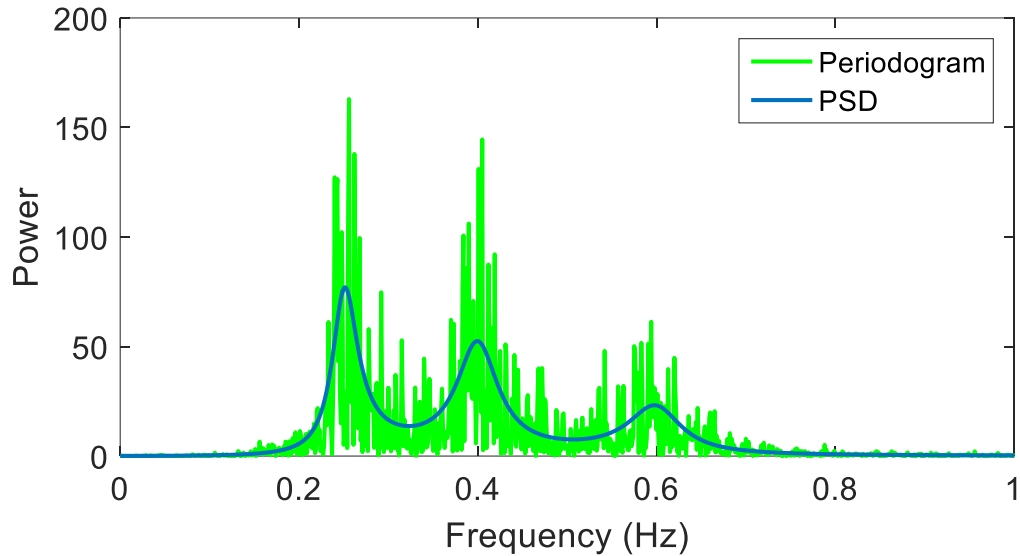


Figure 3-7: Periodogram and PSD of output data from the second area of the example model.

Though many methods of refining the periodogram in Figure 3-7 are available, one of the most common is the Welch periodogram. In Welch's method, the dataset is broken into overlapping segments. A window is applied to each segment before calculating the periodogram. Finally, the periodograms from each segment are averaged to obtain the final estimate. The Welch periodogram in Figure 3-8 was calculated using 1-minute segments with 30 seconds of overlap. The significant reduction in variance compared with the simple periodogram in Figure 3-7 makes the Welch periodogram and other refined periodogram methods useful spectral estimators in practical applications.

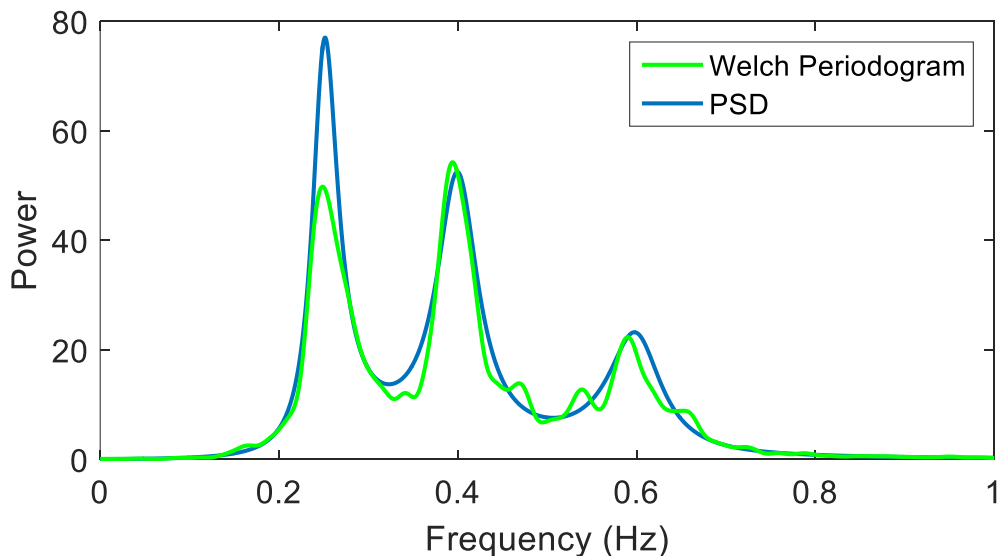


Figure 3-8: Welch periodogram and PSD of output data from the second area of the example model.

■

Refined nonparametric spectral estimates such as the one in Figure 3-8 can be used for more than just subjective evaluations of modes. For example, a method of estimating a mode's damping directly from a spectral estimate based on the width of the associated peak can be found in (Vanfretti, Bengtsson, Peric, & Gjerde, 2012). In (Liu & Venkatasubramanian, 2008), the authors describe how the singular value decomposition (SVD) can be applied to spectral estimates as part of the Frequency Domain Decomposition (FDD) algorithm to estimate modal frequency, damping, and shape. The following section describes other characteristics of modes that can be evaluated with frequency-domain approaches.

Spectral Coherence Estimation

Spectral estimation is perhaps the most fundamental approach to analyzing ambient data in the frequency domain, but it is not the only one. Another useful tool is the spectral coherence, which is also commonly referred to as the magnitude squared coherence. The spectral coherence is a frequency-dependent measure varying between zero and one to indicate how linearly related two signals are. It can be estimated by applying Welch's method of averaging. For each segment in the average, the term

$$\hat{C}_{yz}(f) = \frac{|\hat{\phi}_{yz}(f)|^2}{\hat{\phi}_{yy}(f)\hat{\phi}_{zz}(f)} \quad (26)$$

is calculated, where $\hat{\phi}_{yz}(f)$ is a generalization of (25) such that

$$\hat{\phi}_{yz}(f) = \frac{1}{K} \times DFT\{y(k)\} \times DFT\{z(k)\}^*. \quad (27)$$

Here the superscript * denotes the complex conjugate. The usefulness of the spectral coherence is explored in the following example.

Example 3: Use of the Spectral Coherence Estimate to Distinguish Between Electromechanical Modes

In this example, the attributes of the example model listed in Table 2-1 have been modified. With these new attributes, the PSDs for each output channel were estimated by applying Welch's method to 10 minutes of data. The estimates are plotted in Figure 3-9. In each of the three signals, frequency content is apparent near 0.25 Hz and near 0.5 Hz. Without further information, it would be reasonable to conclude that the system has two dominant electromechanical modes that are observable in all three areas.

Examination of the estimate of the spectral coherence between outputs 1 and 3 in Figure 3-10 helps to reveal the truth. Note that the coherence is large near 0.25 Hz, but it is significantly smaller near 0.5 Hz. This result indicates that the 0.25 Hz mode is common to both areas, but the apparent 0.5 Hz mode in Figure 3-9 is not. The true modes are listed in Table 3-2. Note that the number of modes and mode shapes are identical to the base case for the model; only the frequencies of two modes were changed. As demonstrated in this example, estimates of the spectral coherence can be powerful tools in distinguishing between electromechanical modes with similar frequencies.

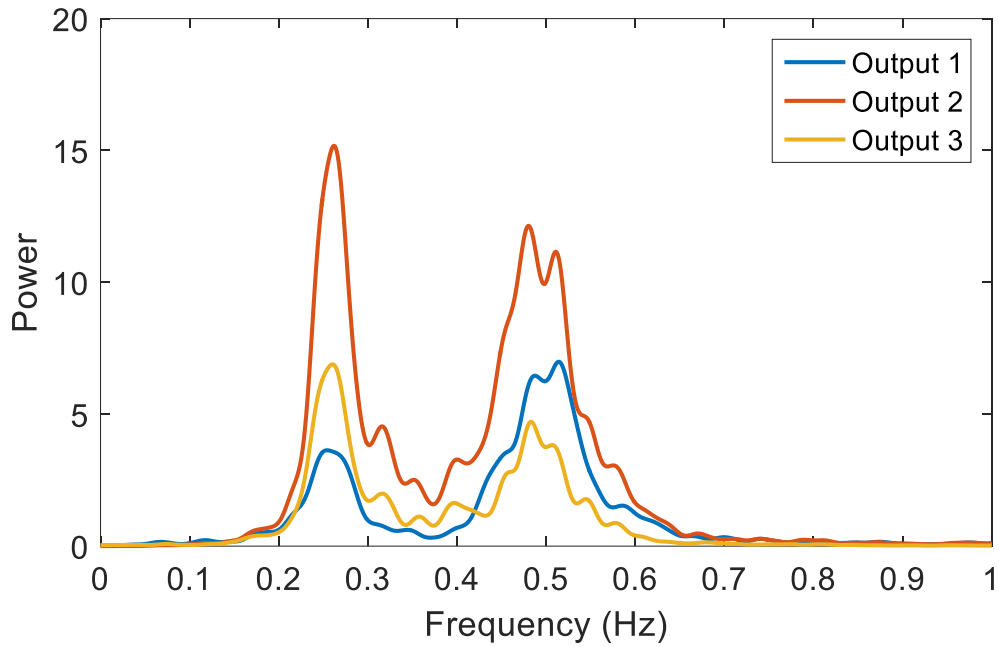


Figure 3-9: Estimates of the PSD for each of the output channels from the modified example model.

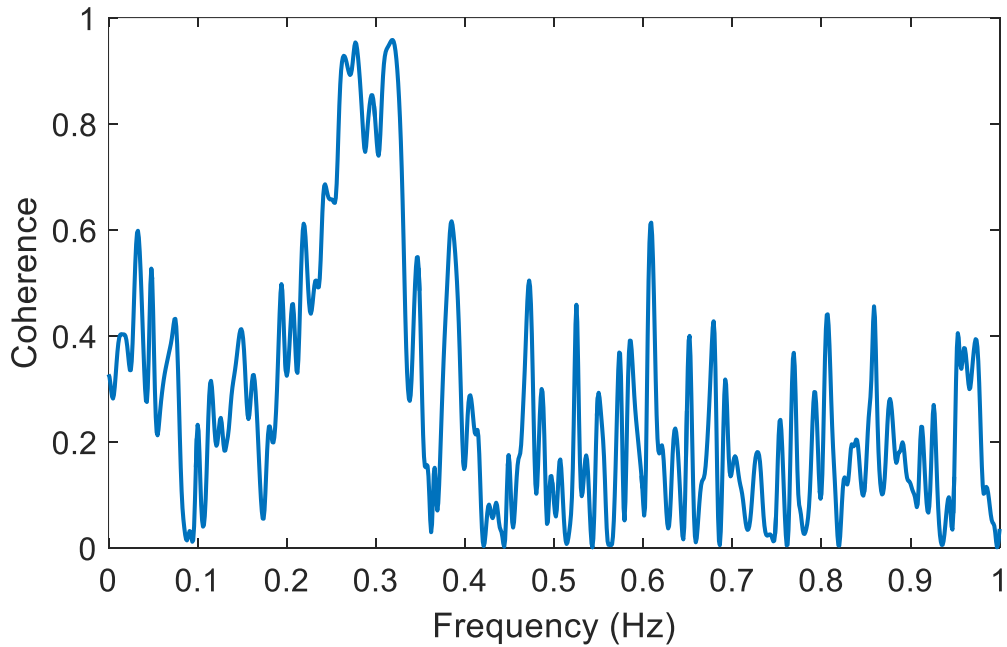


Figure 3-10: Estimate of the spectral coherence between the modified model's first and third outputs. Note the lack of a peak near 0.5 Hz.

Table 3-2. List of electromechanical modes in the modified model used to generate data for Example 3.

Frequency (Hz)	Damping Ratio (%)	Shape	
		Group 1	Group 2
0.25	7	Areas 1 & 3	Area 2
0.5	7	Area 1	Area 2
0.49	6	Area 2	Area 3

■

In practical situations, it is important to distinguish between electromechanical modes, as in Example 3. Some methods of estimating the electromechanical modes perform better when channels with high observability of a specific mode or set of modes are selected for analysis. The estimation problem is made much more difficult when channels with high observability of modes at similar frequencies are included. Clearly distinguishing between a system's modes is also important for the next topic, estimation of mode shape using ambient data.

Mode Shape Estimation

Frequency-domain methods for mode shape estimation include the spectral method (Trudnowski D. , 2008) and the Frequency Domain Decomposition (FDD) method (Liu & Venkatasubramanian, 2008). These methods utilize the non-parametric spectral and spectral coherence estimation methods described in the previous subsections. As demonstrated in (Dosiak, Zhou, Pierre, Huang, & Trudnowski, 2013), the methods are both special cases of the transfer function method (Zhou, Huang, Dosiak, Trudnowski, & Pierre, 2009). Because of its similarities to previous examples, the spectral method will be considered in the following example.

Example 4: Mode Shape Estimation with the Spectral Method

In the example model described in Section 2.4, areas one and three oscillate against area two as dictated by the 0.25 Hz mode. Estimating the shape of this mode with the spectral method described in (Trudnowski D. , 2008) is the focus of this example. Let $\hat{\phi}_{il}(f)$ denote the estimates of the PSD (for $i = l$) and the cross power spectral density (for $i \neq l$) generated by applying Welch's method to (27). In (Trudnowski D. , 2008), the assumption that $\lambda = \sigma + j\omega$ can be approximated as $j\omega$, i.e., the mode of interest has low damping, leads to an estimator for the transfer function in (24). Recalling from Section 2.2.1 that $f = \frac{\omega}{2\pi}$, the mode shape magnitude estimate for output p is

$$|\widehat{MS}_p| = \frac{\hat{\phi}_{pp}(f)}{\hat{\phi}_{RR}(f)} \quad (28)$$

and the mode shape angle estimate for output p is

$$\angle \widehat{MS}_p = \angle \hat{\phi}_{Rp}(f). \quad (29)$$

Because $\hat{\phi}_{pp}(0.25)$ is largest for output two, it is selected as the reference output, i.e., $R = 2$. Results from the application of (28) and (29) to the 10 minutes of ambient data used in previous examples for these selections are plotted in Figure 3-11. From the plot, it is clear that area 2 participates most heavily in the oscillation and oscillates against areas 1 and 3. This result reflects the mode shape listed in Table 2-1.

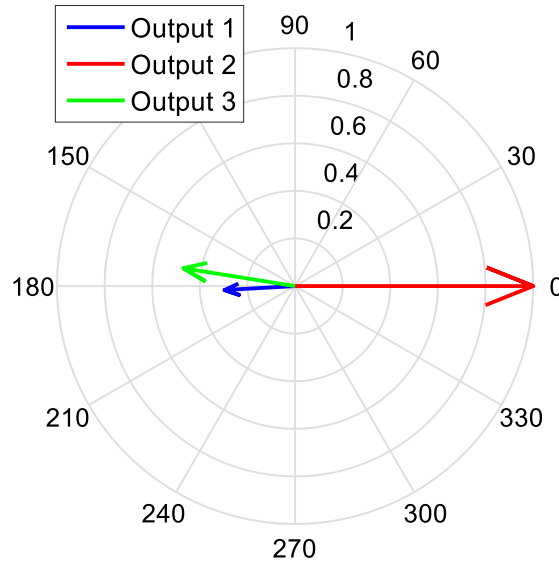


Figure 3-11: Spectral method mode shape estimates based on ambient data from the example model.

Before concluding this example, a comment about the practical implementation of the method must be made. Note that the equations for the spectral mode shape estimator given by (28) and (29) are based on system measurements, but mode shape is defined for power system states that are not measured by PMUs, e.g., generator shaft speed. Measurement-based mode shape estimators often rely on the assumption that only measurements collected near generator terminals and consequently dominated by a system state are used in the analysis.

■

3.2. Transient Response

Power system transient responses fall within the larger class of natural oscillations. Though sharing this categorization with ambient noise, their appearance in time-domain data is significantly different, as is demonstrated in Figure 3-12 using the example model. As a result, techniques specific to their analysis have been developed. Transient responses were studied before ambient noise, and there is a wealth of literature published on the topic. In this section, the sources, characteristics, and proper analysis techniques associated with transient responses will be described.

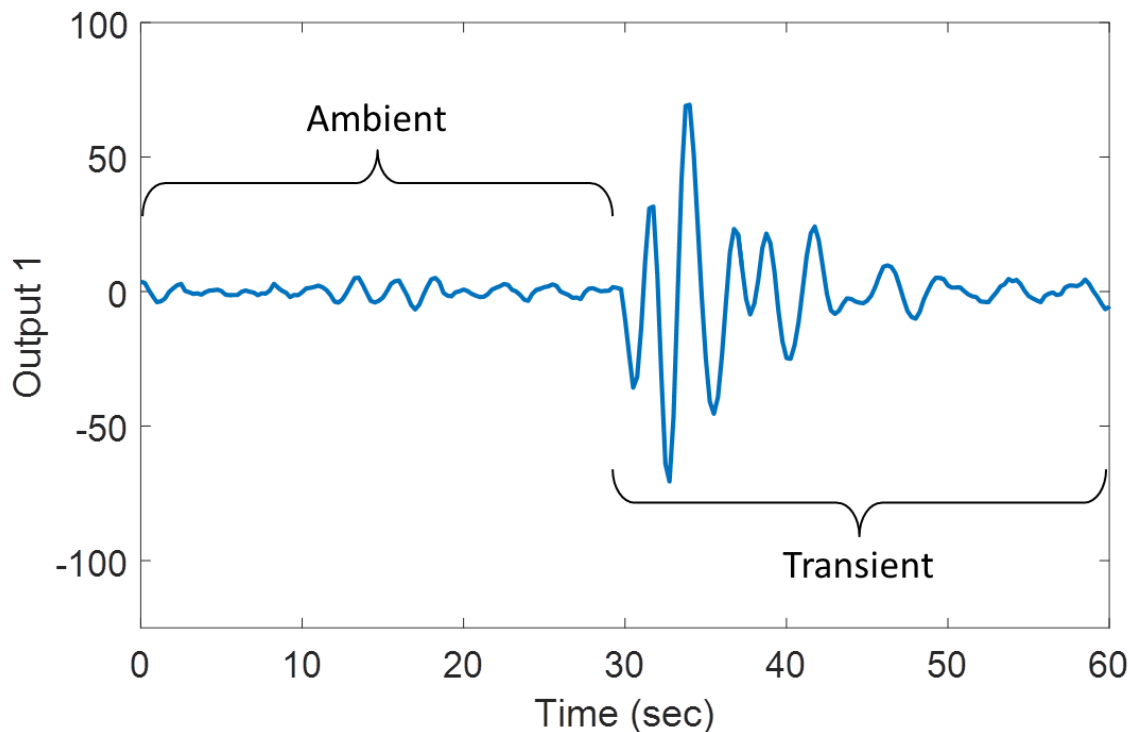


Figure 3-12: Ambient and transient data from the example model.

3.2.1. Sources of Transient Responses

In contrast to a power system's ambient response, which is constantly present due to random low-level system disturbances, transient responses are initiated by system events and die out over short time intervals. The scale and type of the event can vary significantly. For example, faults and trips on transmission lines, the sudden loss of generation, and load tripping can all cause transients visible at the transmission level of a power system. When these events occur, they act as a large, sudden excitation to the system. The transient response describes how the system settles back to a steady state condition following such an excitation.

To understand how events impact the system and how the resulting transient responses can be analyzed, it is helpful to describe these events as system inputs. As an example, consider an unscheduled generator trip. Because this constitutes a sudden, large, and long-lasting change, it can be thought of and modeled as a step change. Though the example model described in Section 2.4 is not detailed enough to model a generator trip, application of a step change does result in a response similar to those observed in power systems following a generator trip, as can be seen in Figure 3-13. Note that the input also contains a random component that results in ambient noise. As a second example, consider a lightning-induced fault on a transmission line that is cleared after a single operation of a recloser. This event can be thought of and modeled as an impulse because it impacts the system for a short time and afterward the system returns to the conditions that existed before the fault. The impulse input and resulting output of the example model are plotted in Figure 3-14.

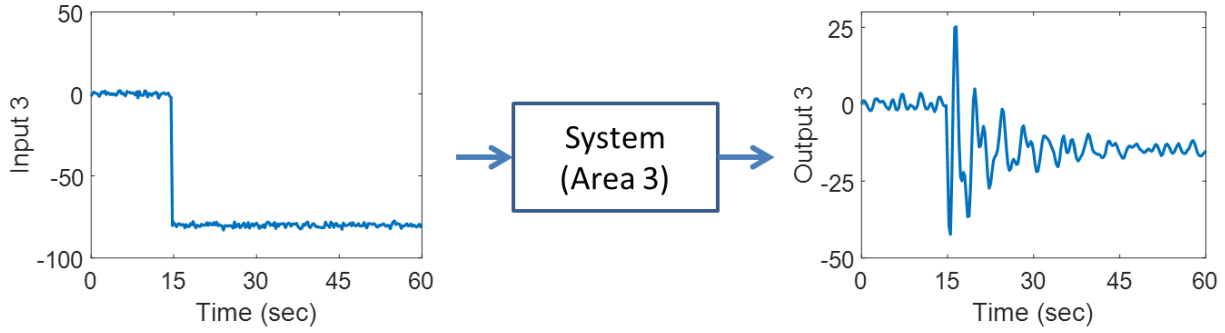


Figure 3-13: Response of the example system's third output to a step change at input 3.

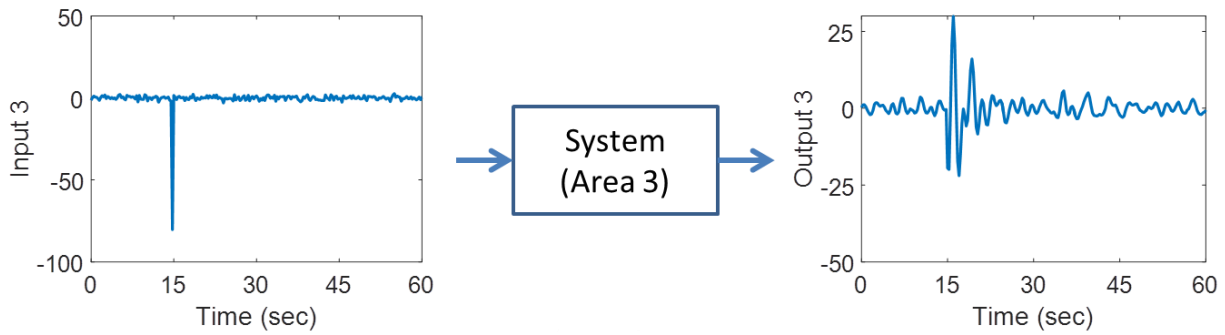


Figure 3-14: Response of the example system's third output to an impulse at input 3.

Whether the event is better characterized as a step change or an impulse, the resulting “ringdowns” in Figure 3-13 and Figure 3-14 are characteristic of transient responses. One component of this response reflects the input and one component reflects the system (Kamen & Heck, 2007). In power systems, as is generally true with other systems, it is the oscillatory behavior apparent in a ringdown resulting from a step or impulse input that is associated with the characteristics of the system. This relationship makes it possible to determine information about the power system by analyzing ringdowns. Before discussing analysis techniques, the characteristics of transient responses and their relation to the system's characteristics will be described in the following section.

3.2.2. Characteristics of Transient Responses

The transient responses depicted in Figure 3-13 and Figure 3-14 can be characterized in continuous time as a sum of damped sinusoids, i.e.,

$$y(t) = \sum_{m=1}^M 2e^{\sigma_m t} |C_m| \cos(\omega_m t + \angle C_m) \quad (30)$$

where M is the number of dominant inter-area electromechanical modes and the C_m are complex valued scalars known as residues. As before, $\lambda_m = \sigma_m + j\omega_m$ is a continuous-time eigenvalue corresponding to a dominant electromechanical mode. A single term in (30) corresponding to the 0.4 Hz mode in the example model is plotted in Figure 3-15 for $C_m = 1$. The frequency of the

sinusoid (gray) and damped sinusoid (black) are equal to the mode's frequency of 0.4 Hz. The decay of the damped sinusoid's amplitude is driven by the exponential, particularly σ_m . The decay will occur quickly for $\sigma_m \ll 0$, i.e., when the mode is very stable, and slowly as σ_m approaches 0. When σ_m equals 0, the exponential term becomes unity and the undamped sinusoid (gray in Figure 3-15) will be present in the transient response. If σ_m is greater than 0, the system is unstable and the oscillation will grow without bound as depicted in Figure 3-16.

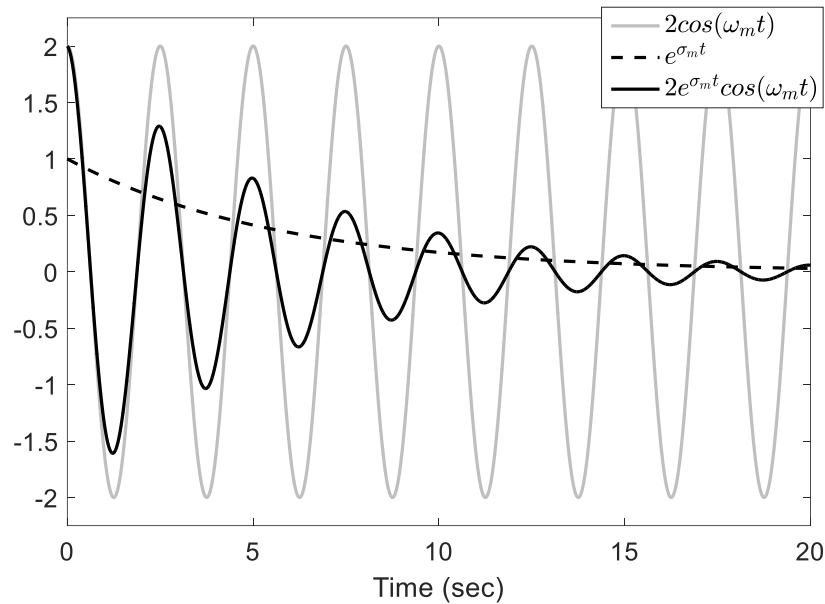


Figure 3-15: Transient response term for $\sigma_m = -0.176$, which leads to a damping ratio of 7%. In regard to this mode, the system is stable.

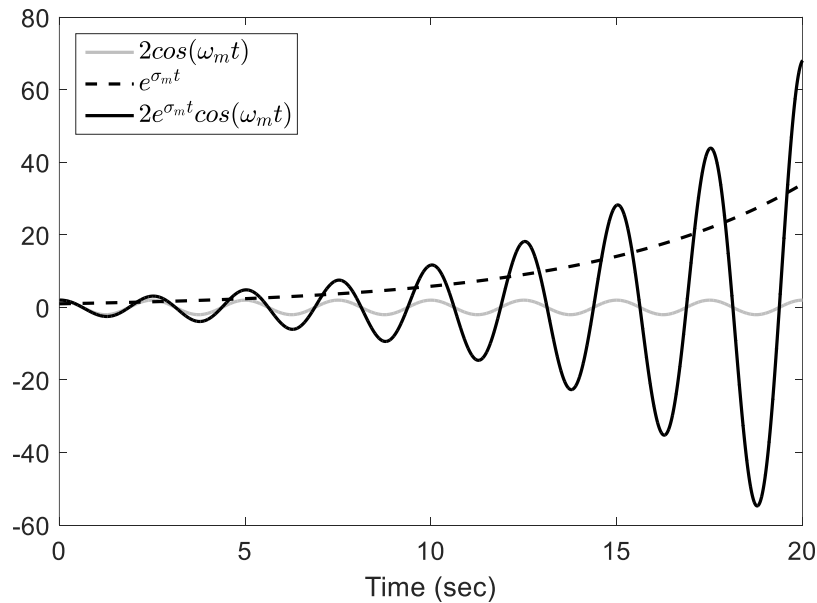


Figure 3-16: Transient response term for $\sigma_m = 0.176$, which leads to a damping ratio of -7% and unstable system conditions.

As is clear from (30), the residue term C_m dictates the amplitude and phasing for each damped sinusoid. Whereas λ_m is identical for a mode no matter where a measurement is taken, the residue for each mode varies throughout the system. At measurement locations where the mode is highly observable, the residue will be large. The residue's angle will be similar for areas swinging together and nearly 180° apart for areas swinging against each other. Thus, a mode's residues are closely related to its shape. The fact that the parameters of the system's dominant modes dictate the form of the transient response leads to the analysis methods described in the following section.

3.2.3. Analysis of Transient Responses

After a significant event disturbs the power system, the system's return to steady state is dictated by the transient response. Typically characterized as a natural response, the form of a transient response reflects the system's electromechanical dynamics. Thus, the transient response can be analyzed to estimate the properties of the system's electromechanical modes. Due to the large signal-to-noise ratio afforded by significant transient responses, analysis methods properly applied to ringdowns tend to provide more accurate estimates than their ambient analysis counterparts.

There are two general approaches specific to analyzing power system transients to obtain estimates of the electromechanical modes. One of these approaches is to fit a low-order state-space model based on the measured ringdown. Examples of this approach are the Minimal Realization Algorithm (Kamwa, Grondin, Dickinson, & Fortin, 1993) and the Eigensystem Realization Algorithm (Sanchez-Gasca & Chow, 1997). The alternative approach is to fit a sum of sinusoidal, or equivalent exponential, terms to the response described by (30). Methods that fall into this category include the Prony (Hauer, Demeure, & Scharf, 1990) (Trudnowski, Johnson, & Hauer, 1999), Matrix Pencil (Liu, Quintero, & Venkatasubramanian, 2007), Hankel Total Least Squares (Liu, Quintero, & Venkatasubramanian, 2007), and Variable Projection (Borden, Lesieutre, & Gronquist, 2013) algorithms. Before examining this approach further, it should also be mentioned that some ambient analysis techniques can be successfully applied to ringdown data, an important quality in practical applications where continuous monitoring is desired. However, the opposite is generally not true. Algorithms specific to transient responses will not provide accurate results when applied to ambient data because ambient data cannot be well described by (30).

Example 5: Analysis of a Transient Response with Prony's Method

In this example, Prony's method is used to estimate the modes of the example model by analyzing ringdowns in the model's outputs. The transient response is initiated by a half-second pulse applied to input 2 to reflect the insertion of the Chief Joseph dynamic brake in the western North American Power System (wNAPS) for testing purposes. As can be seen in Figure 3-17, the pulse resulted in transients in each of the model's outputs.

Selecting a proper window of data for analysis is important for all methods applied to transients. There are two primary considerations: 1) linearity of the system and 2) SNR of the measurements. Everything discussed in this section assumes that the system generating the transient response exhibits linear behavior. Though power systems are in reality nonlinear systems, they tend to behave linearly about an operating point. When the

operating point changes dramatically, as happens during a system event, the initial portion of the response cannot be characterized as linear. Thus, a good rule of thumb is to exclude the first two swings of the response if the transient is large. For the second consideration, it is important to remember that transient analysis methods are applicable to signals composed of a sum of sinusoids. Thus, it is important to include only portions of data where the transient response is dominant. The window used for analysis is highlighted in black for output 2 in Figure 3-18.

Results from the analysis of the ringdowns in Figure 3-17 with the multi-channel Prony method described in (Trudnowski, Johnson, & Hauer, 1999) with a model order of 12 are listed in Table 3-3 and Table 3-4. Mode estimates corresponding to true modes are listed in bold with true values in parenthesis. The mode shape estimates in Table 3-4 are obtained by normalizing estimates of the residues. Comparison with Table 2-1 indicates that, for a given mode, outputs with large mode shape magnitudes are strong participants in the mode and those with opposing mode shape angles swing against each other.

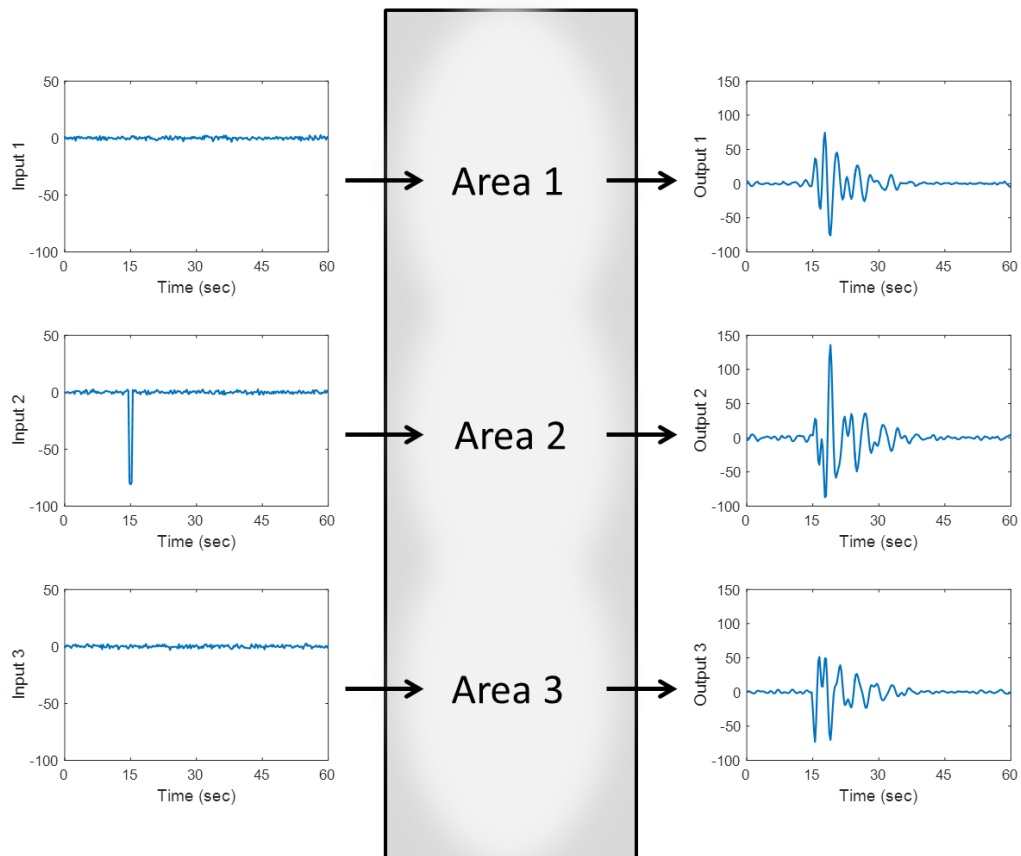


Figure 3-17: Inputs to the example model and the resulting transient responses apparent in the model's outputs.

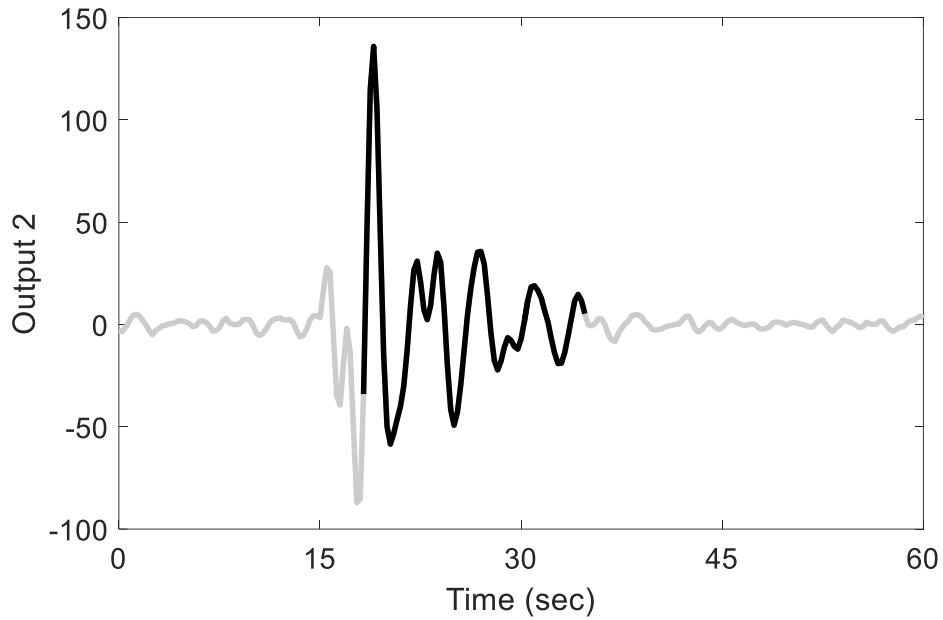


Figure 3-18: Portion of data from output 2 used for analysis (black).

Table 3-3. Mode estimate results from application of Prony's method to modeled data. Estimates corresponding to true modes are listed in bold with true values in parenthesis.

Frequency (Hz)	Damping Ratio (%)	Pseudo-Energy (Normalized)
0.250 (0.25)	6.578 (7)	1.000
0.403 (0.4)	7.066 (7)	0.564
0.597 (0.6)	5.643 (6)	0.166
1.843	6.505	0.5029×10^{-4}
1.037	4.982	0.2723×10^{-4}
1.475	4.892	0.0482×10^{-4}

Table 3-4. Mode shape estimates from application of Prony's method to modeled data. Estimates corresponding to true modes are listed in bold. All estimates have been normalized using output 2 as reference.

Output 1	Output 2	Output 3
0.50 \angle 174.2°	1.00 \angle 0.0°	0.70 \angle -165.9°
0.90 \angle 174.5°	1.00 \angle 0.0°	0.25 \angle -163.7°
0.33 \angle 117.8°	1.00 \angle 0.0°	0.72 \angle 168.2°
0.66 \angle 142.6°	1.00 \angle 0.0°	0.42 \angle -127.8°
0.35 \angle 118.0°	1.00 \angle 0.0°	0.40 \angle 156.6°
0.17 \angle 132.8°	1.00 \angle 0.0°	0.75 \angle -160.6°

The pseudo-energy listed in Table 3-3 is a metric for how much each estimated mode contributes to the input signals. Recall from (30) that transients are modeled as sums of damped sinusoids. The six damped sinusoids for output 2 corresponding to the mode estimates in Table 3-3 are plotted in Figure 3-19. The sum of these damped sinusoids leads to the modeled signal depicted in Figure 3-20. Good agreement between the measured and modeled signals is an indicator that the model is capturing the dominant modes at the measurement location.

In Figure 3-19, note that the three damped sinusoids corresponding to the true modes are much larger than the others and thus contribute more to the transient. The pseudo-energy for the m^{th} mode estimate is given by

$$E_m = \sum_{r=1}^R \sum_{k=k_1}^{k_2} |\hat{y}_{r,m}(k)|^2 \quad (31)$$

where R is the number of channels, the indices of the analyzed portion of the signal are given by $k_1 \leq k \leq k_2$, and $\hat{y}_{r,m}(k)$ denotes the damped sinusoid associated with the m^{th} mode estimate for channel r . The small values for pseudo-energy given in Table 3-3 for the final three entries indicate that those mode estimates do not correspond to the system's dominant electromechanical modes. Still, their inclusion improves the estimation by capturing noise terms and higher frequency components.

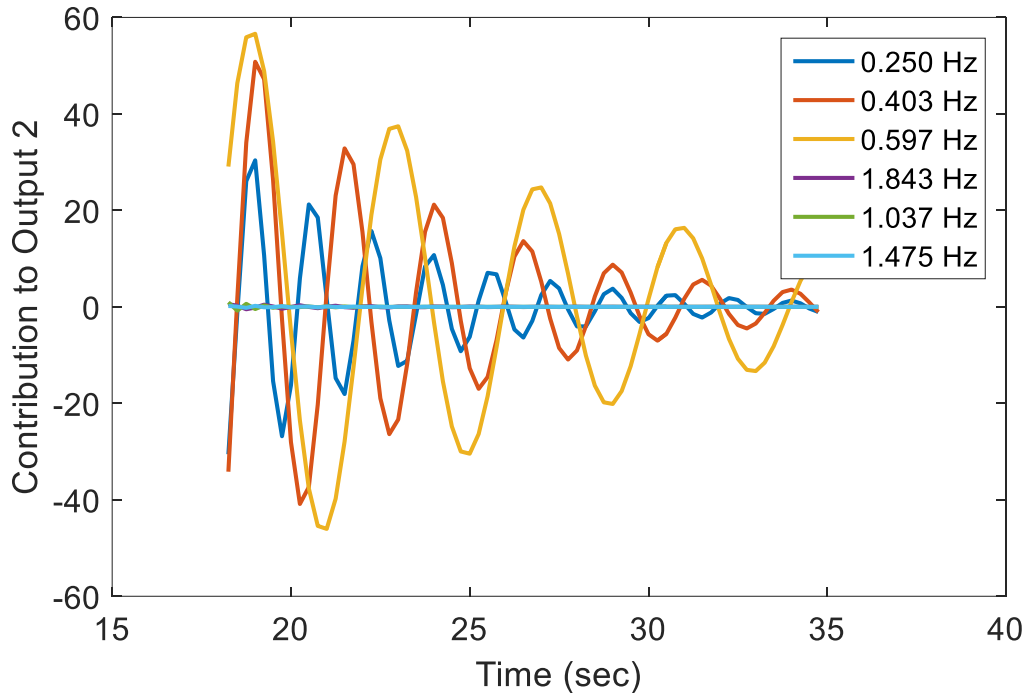


Figure 3-19: Estimated contribution of the damped sinusoids associated with each mode in Table 3-3 to the transient in output 2.

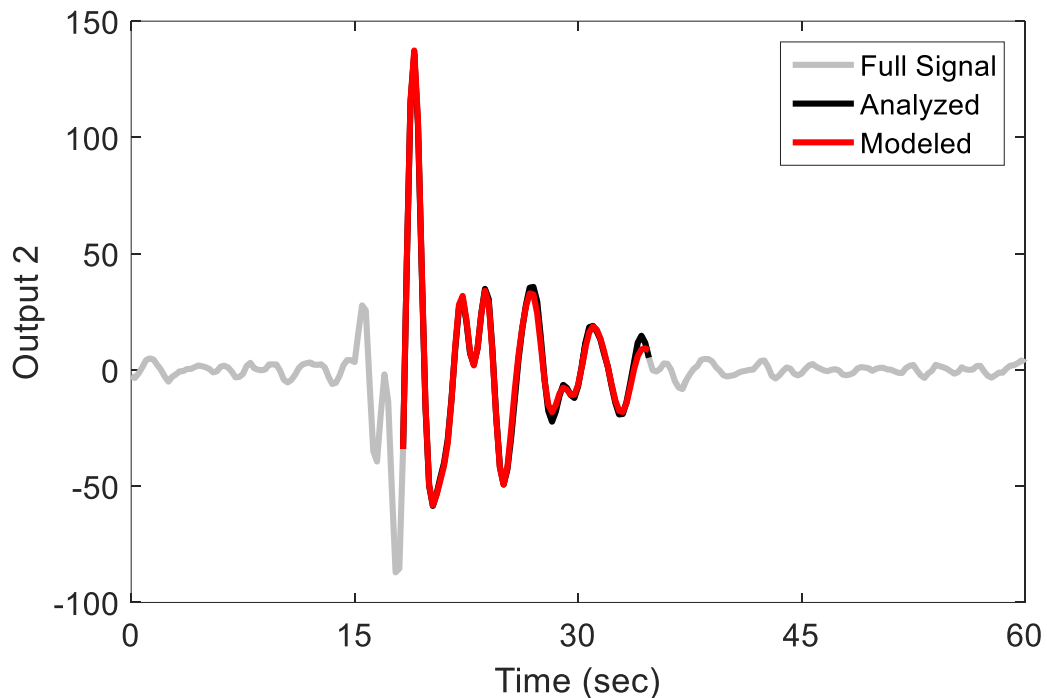


Figure 3-20: The signal used for analysis (black) and the modeled signal based on the mode estimates (red) for output 2.

As mentioned previously, the strong agreement between the measured and modeled signals in Figure 3-20 is an indicator that the dominant modes are being captured. However, caution must be taken. By increasing the model order to 22, a slightly better fit can be achieved and the estimates in Table 3-5 are obtained. Note that the estimates in bold are both near the frequency of a system mode. Though the pseudo-energy of the 0.282 Hz component is much smaller, it still contributes significantly to the modeled signal, as can be seen in Figure 3-21. This occurrence is known as mode splitting. It occurs when the selected model order is too high, causing the contribution from a true electromechanical mode to be split between two estimated modes. For this reason, it is good practice to select the smallest model order that provides a sufficiently good fit between measured and modeled data by capturing the contributions of each dominant mode.

Table 3-5. Mode estimate results from application of Prony’s method to modeled data with a high model order of 22. The “split mode” estimates are highlighted in bold font.

Frequency (Hz)	Damping Ratio (%)	Pseudo-Energy (Normalized)
0.249	7.689	1.000
0.398	6.778	0.492
0.598	4.800	0.125
0.282	14.019	0.034
1.149	10.016	0.857×10^{-3}
1.262	12.522	0.569×10^{-3}
0.964	8.389	0.396×10^{-3}
0.780	4.604	0.043×10^{-3}
1.918	2.209	0.012×10^{-3}
1.476	2.365	0.006×10^{-3}
1.681	2.132	0.002×10^{-3}

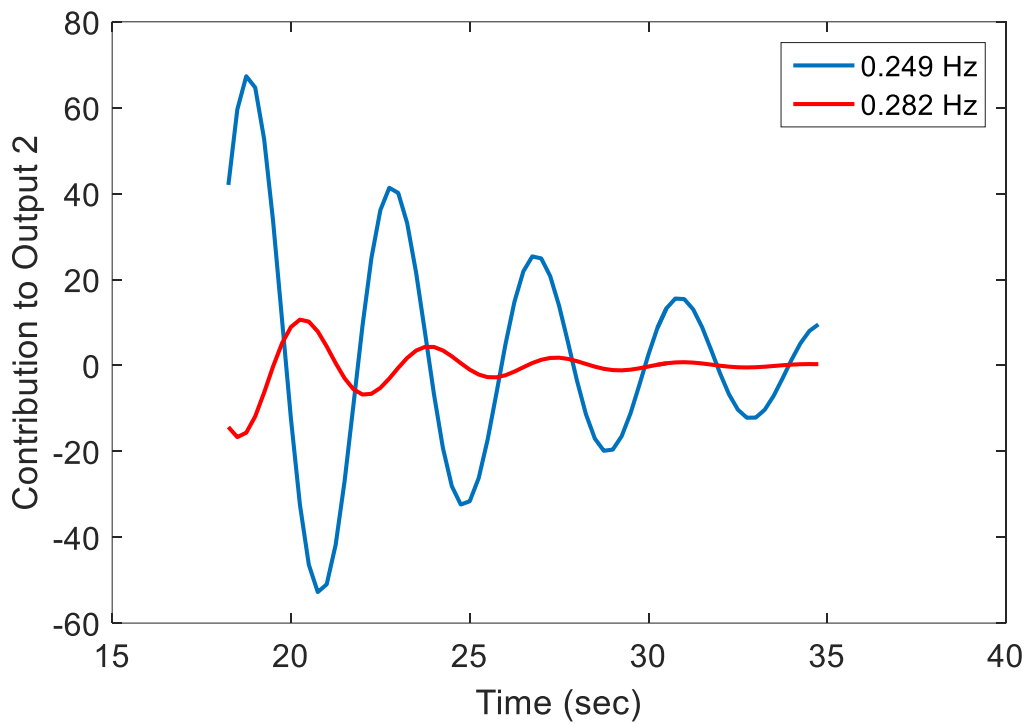


Figure 3-21: Estimated contribution of the damped sinusoids from the split mode listed in Table 3-5 to the transient in output 2.

■

4. Forced Response Oscillations

Recall that system responses can be characterized by natural and forced components. Natural components often used in modal analysis were discussed in Section 3. In this section, the sources and characteristics of forced responses, along with analysis approaches, are described. The distinction between natural and forced oscillations is an important one. The proper response of power system engineers and operators to a forced oscillation is different than that of a modal oscillation. Further, using analyses meant for one type of oscillation on the other can be misleading. To understand why, the sources of forced oscillations must be examined.

4.1. Sources of Forced Responses

Forced oscillations have a wide variety of sources spanning cyclic loads, equipment, and thermal-, hydro-, diesel-, and renewable-generation plants. Despite this tremendous variety, these components can impact the system in similar ways that lead to forced oscillations. Specifically, they are able to introduce periodic disturbances to the system that can, under certain circumstances, be observed across the system.

It should be noted that the discussion in this document is limited to “true” forced oscillations and does not extend to limit cycles associated with Hopf bifurcations. Though sustained oscillations associated with limit cycles can display similar characteristics as forced oscillations, their existence is tied to system dynamics and stability in a way that forced oscillations are not. The distinction between these types of oscillations is recognized in (Wang & Turitsyn, 2016) and (Xie & Trudnowski, 2015). For details on oscillations related to limit cycles and Hopf bifurcations see (Wang & Turitsyn, 2016) and the references therein. This document is also limited to forced oscillations with distinct periods because methods for analyzing and modeling forced oscillations driven by a narrowband input, e.g., a hydro-generating unit running in the rough zone, are not yet well established.

As mentioned previously, forced oscillations can be introduced by cyclic loads, equipment, or generation plants. Examples of cyclic loads include nuclear accelerators (Pinneilo & Van Ness, 1971), steel plants, cement mills, and aluminum processing plants (Rao & Jenkins, 1988). While cyclic loads tend to introduce oscillations while operating properly, equipment and generating units that produce unintentional oscillations tend to do so because of a malfunction in control or a physical component (Myers & Trudnowski, 2013) (Silverstein, 2015). The oscillations resulting from such malfunctions can be viewed as periodic system inputs with a variety of waveforms, e.g., sawtooth, pulse train. This periodic nature is preserved in forced oscillations as they pass through the system and are measured at system outputs. Because these outputs reflect the characteristics of an input rather than the system, they are part of the system’s forced response. Further details are provided in the following section.

4.2. Characteristics of Forced Responses

Due to the variety of forced oscillation sources, the characteristics of these oscillations can vary greatly. Some forced oscillations are large enough to be apparent in time domain measurements, while others would go unnoticed in PMU measurements without careful examination. An example of a real-world forced oscillation that, after preprocessing, is apparent in time-domain data is presented in Figure 4-1. Similar examples can be found in (Silverstein, 2015),

(Trudnowski D. , Pierre, Donnelly, & Venkatasubramanian, 2015), and (Myers & Trudnowski, 2013). In this section, the characteristics that are common to the wide range of forced oscillations are discussed.

To describe the characteristics of forced oscillations as they are observed in measurements, it is helpful to begin with the inputs that create them. Due to the periodic nature of these inputs, they can be expressed with the Fourier series as

$$u(t) = \alpha_0 + \sum_{h=1}^{\infty} \alpha_h \cos(h\omega_0 t + \theta_h) \quad (32)$$

where ω_0 is the fundamental frequency with units of radians per second (Kamen & Heck, 2007). Each term in the sum is a harmonic. This expression is quite general in that $u(t)$ can be any periodic waveform, e.g., pulse train, sawtooth, or multisine. For the reasons described next, forced oscillations often do not reflect this waveform when measured at a system output.

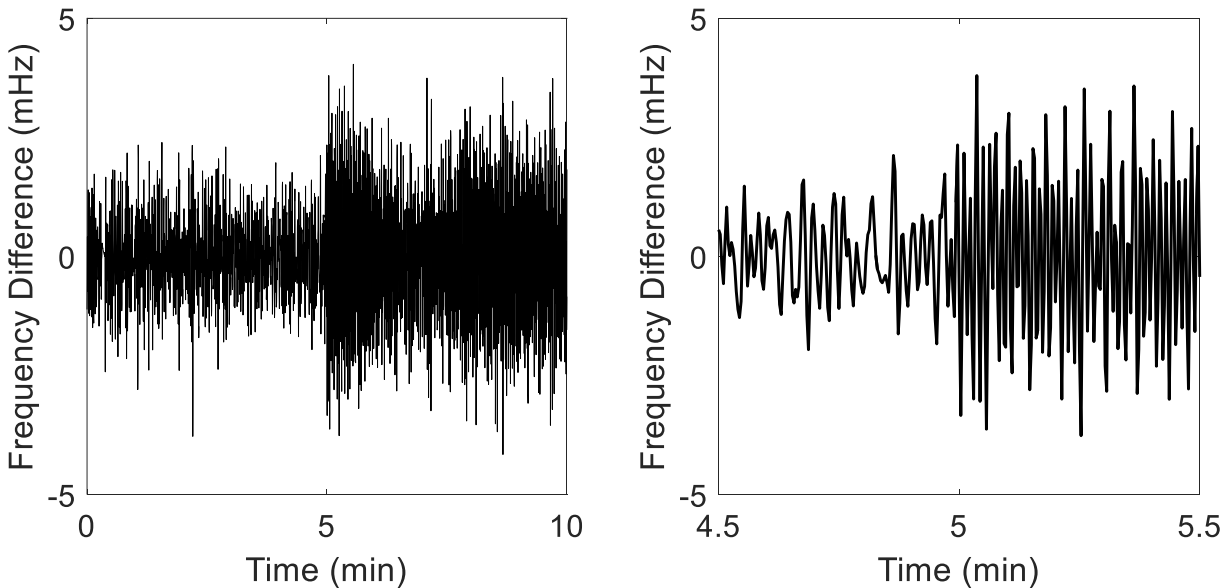


Figure 4-1: Real-world example of a forced oscillation apparent in time-domain PMU data.

Forced oscillations do not arise because of the system's dynamics, but they are influenced by them. Letting $G_i(\omega)$ denote the transfer function between the forced oscillation's input and the output i , the component of the measured output corresponding to the forced oscillation can be expressed as

$$y_{i,u}(t) = G_i(0)\alpha_0 + \sum_{h=1}^{\infty} |G_i(h\omega_0)|\alpha_h \cos(h\omega_0 t + \theta_h + \angle G_i(h\omega_0)). \quad (33)$$

Note that the amplitude of each harmonic component is scaled in amplitude and shifted in phase based on the transfer function. As a result of this scaling and shifting, the measured output will generally not have the same time-domain appearance as the input. However, it does have the same frequency components. The presence of harmonics is a strong indicator that a power

system oscillation is forced, rather than natural. These characteristics are illustrated in the following example.

Example 6: Effect of System Dynamics on a Forced Oscillation's Characteristics

For this example, a square wave with unit amplitude was added to the example model's third area to induce a forced oscillation. The first several Fourier series coefficients for this square wave are given in Figure 4-2 as a function of harmonic frequency. Note that all coefficients for even harmonics are equal to zero.

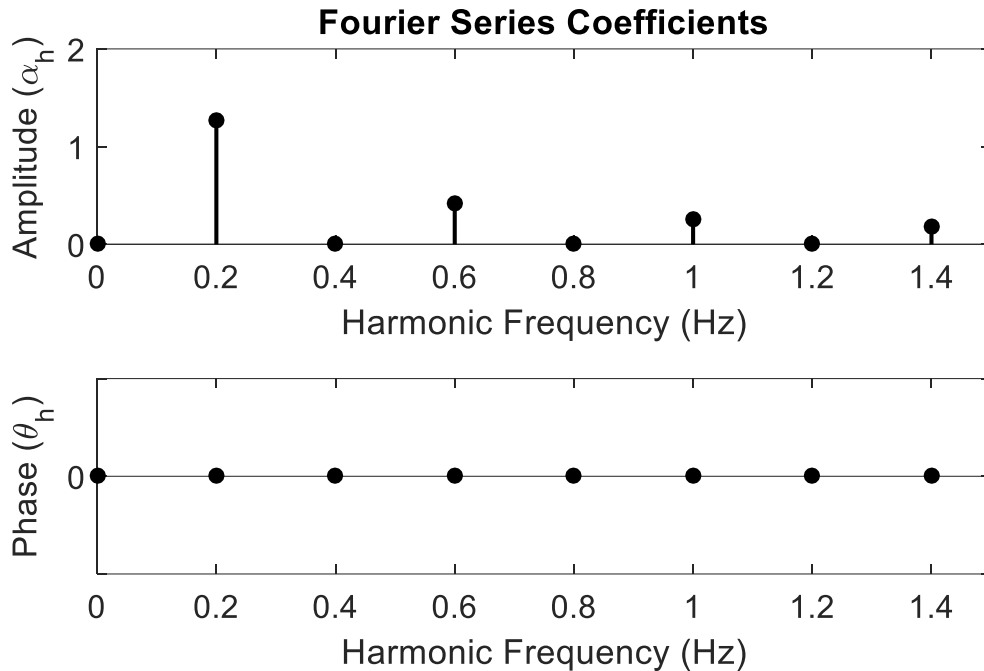


Figure 4-2: Fourier series coefficients of the 0.2 Hz square wave input to the example model's third area to induce a forced oscillation.

The forced oscillation that results from the square wave input can be seen in all three of the model's outputs, but here the output from area 2 is considered. The frequency response of the system from input 3 to output 2 is plotted in Figure 4-3. Values at frequencies corresponding to the odd harmonics of the input square wave are indicated in the plot. When the square wave passes through the system from input 3 to output 2, a gain and phase shift are applied to each of the frequency components in Figure 4-2. Recall that these coefficients correspond to the sinusoids in (32). The first several Fourier series coefficients for the forced oscillation portion of output 2 that result from the gain and phase shift are depicted in Figure 4-4. Note that due to the large gain at 0.6 Hz (see Figure 4-3), the largest Fourier series coefficient in the output corresponds to the third harmonic.

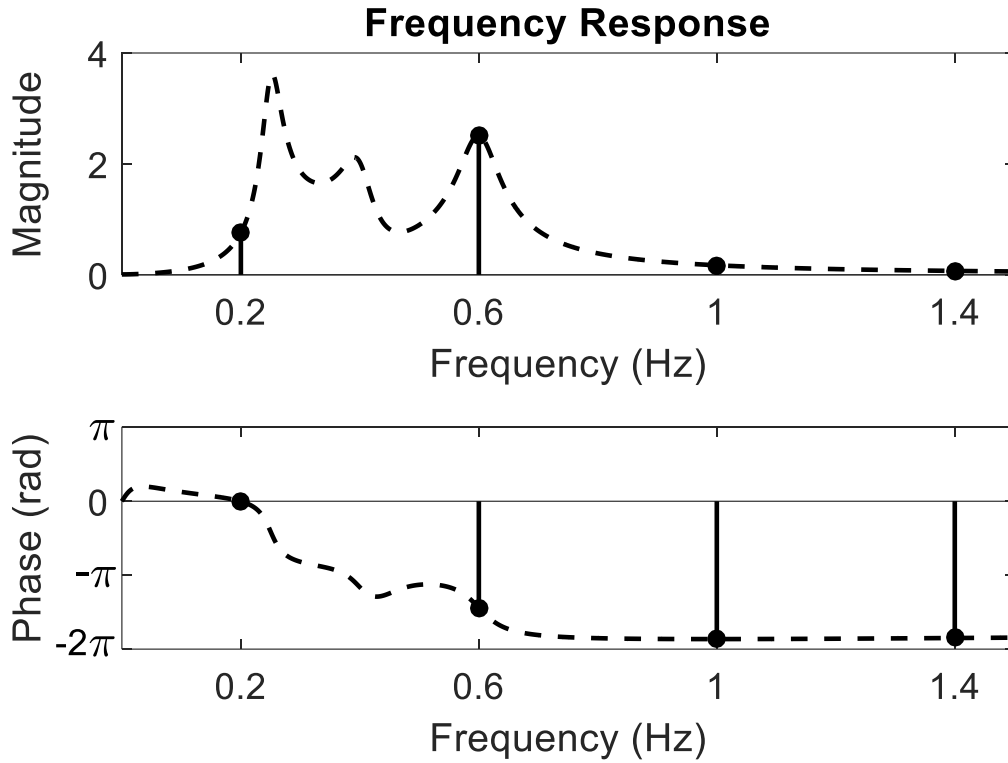


Figure 4-3: Frequency response of the example system from input 3 to output 2.

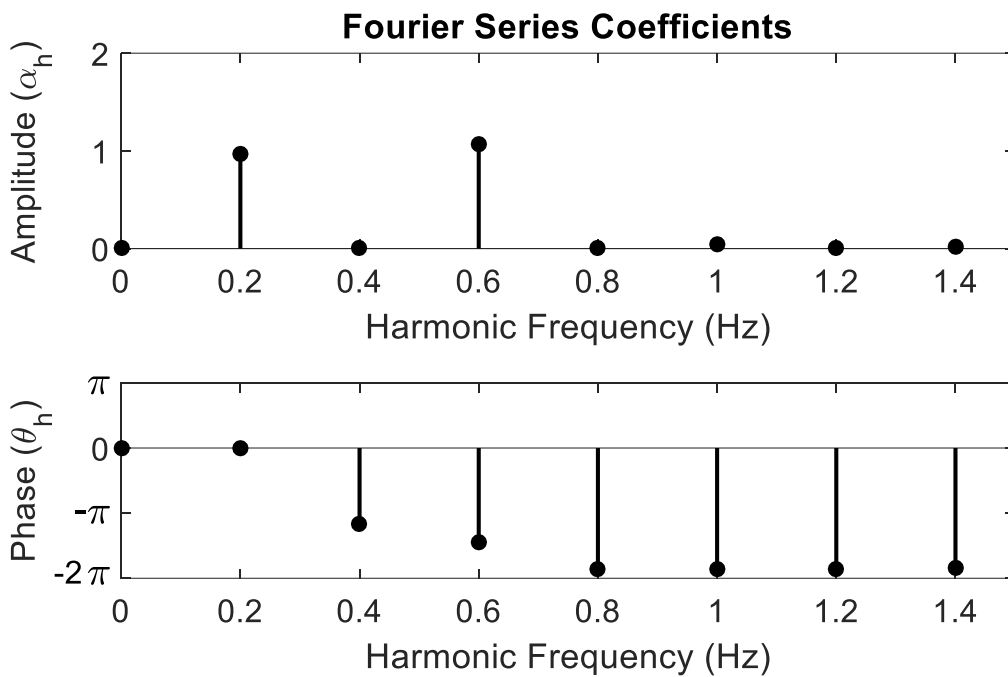


Figure 4-4: Fourier series coefficients for the forced oscillation portion of output 2.

The gain and phase shifts dramatically impact the shape of the forced oscillation as it appears in output 2, as is apparent in Figure 4-5. In the figure, the waveform could clearly be described as a sum of sinusoids. When output 2, including both the forced oscillation and ambient noise portions, is analyzed in the frequency domain, the component sinusoids are apparent. The spectral estimate in Figure 4-6 was obtained by applying a Welch periodogram to the output from area 2. Along with the ambient noise spectrum, line spectra, which are indicative of sinusoidal signal components, are apparent at the odd harmonics of 0.2 Hz. These are the exact same frequency components in the input signal (see Figure 4-2). The spectral estimate in Figure 4-6 is reflective of those obtained from actual PMU data. As a forced response of the system, the forced oscillation measured at the system's output retains the characteristics, in this case the frequency components, of the input that induced it. For this reason, the presence of harmonics is a strong indicator that an observed oscillation is forced, rather than natural. The harmonics that are present, along with the extent to which they are present, depend on the input's particular waveform and the gain between the input and the measured output.

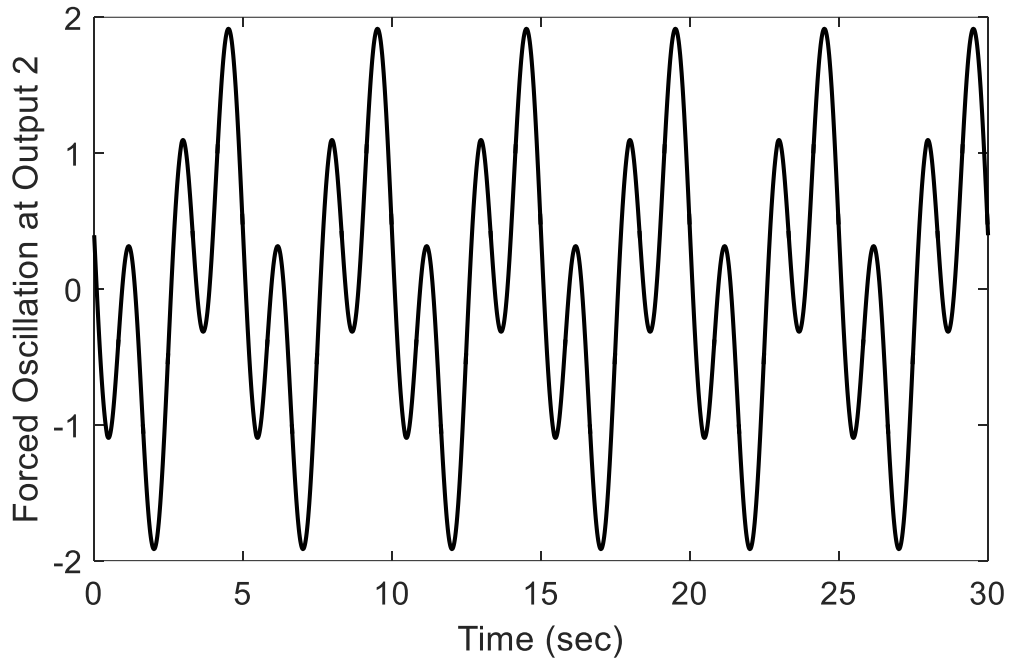


Figure 4-5: Forced oscillation portion of the output from the test model's second area.

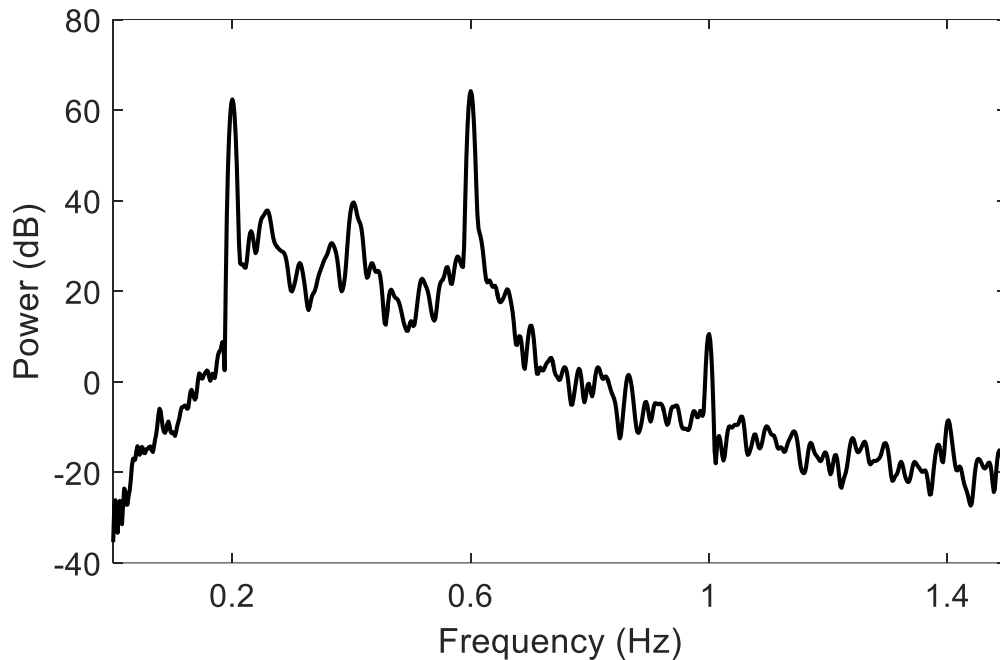


Figure 4-6: Welch periodogram of the output from the test model's second area. Peaks corresponding to forced oscillation frequencies are apparent at odd harmonics of the input oscillation's 0.2 Hz fundamental frequency.

■

While the harmonic content of forced oscillations displayed in the previous example clearly distinguishes them from natural oscillations, other differences are more subtle. For example, it is an important characteristic of forced oscillations that they do not exhibit damping the way natural oscillations do. Note that the description of a transient response in (30) contains the term $e^{\sigma t}$, but the description of a forced oscillation response in (33) does not. Though not conclusive, the undamped characteristic of forced oscillations can help identify them because undamped natural oscillations are rare.

Because forced oscillations tend to be undamped, it can lead to confusion to assign a damping value to an observed forced oscillation. As was discussed in Section 3, the damping of natural oscillations is directly tied to the system's stability. Forced oscillations, though, do not inherit their undamped characteristic from the system, but rather from the driving input. Thus, care must be taken when discussing forced oscillations to clearly distinguish between their damping of zero and the damping of system modes, the two of which are unrelated. Further, estimating the damping ratio of a forced oscillation can be viewed as analogous to fitting linear data to the model

$$y = ax^2 + bx + c.$$

The quadratic coefficient being very near zero indicates that the data is truly linear, but the value itself has little meaning because it is an unnecessary addition to the model. Similarly, a very small damping ratio estimate for an oscillation may indicate that it is forced, but once the

oscillation is known to be forced reporting a specific value for the damping provides little if any information. It should be noted that though forced oscillations are undamped, they may have amplitudes that vary with time due to changes in the driving input. In most cases, this variation cannot be well described using a damping term.

The amplitude and phase of a forced oscillation also vary geographically or, perhaps more accurately, topologically. Oscillations can travel great distances across transmission lines and through transformers. The gain and phase shift applied to a forced oscillation as it passes through the system are dependent on the path that it travels. As a result, PMU measurements of a forced oscillation from different points in the system will have differing amplitudes and phases. An oscillation's variation across a system is often described by its shape.

In (Trudnowski D. , Pierre, Donnelly, & Venkatasubramanian, 2015), oscillation shape is defined as:

...the relative perception of an oscillation at different parts of a power grid. An Oscillation Shape is characterized by the amplitude and phase of a particular frequency component within an oscillation. The Oscillation Shape is unique to the measurement point within the system.

Note that this general definition is based entirely on the observation of an oscillation. When more specifically discussing oscillatory mode shape, the authors of (Trudnowski D. , Pierre, Donnelly, & Venkatasubramanian, 2015) point out that the mode shape is mathematically characterized by the right eigenvector of the system's state matrix (see Section 2.2.1). Thus, mode shape is a property of the system. A forced oscillation's shape is determined in part by the gain and phase shift applied by the dynamics of the system, but it is not a characteristic of the system itself. Thus, the general definition above, which focuses on the relative perception of an oscillation throughout the system, is appropriate for the discussion of a forced oscillation's shape. Examples of a forced oscillation's shape are provided in the following example.

Example 7: Forced Oscillation Shape

In this example, a sinusoidal forced oscillation with unit amplitude is applied at the inputs of the example model. Time-domain plots include only the portion of the response related to the forced oscillation, i.e., ambient noise is excluded for clarity. The associated oscillation shape plots have been normalized so that the channel with the largest amplitude is the reference with unit magnitude and zero phase. Normalization is common in practical applications because the relative shape of the oscillation at various points throughout the power system is of interest.

First, a 0.2 Hz sinusoid is applied to the input of the model's second area. The forced oscillation component of the response at each of the model's output is plotted in Figure 4-7 and the shape is plotted in Figure 4-8. Note that the relative amplitudes and phasing apparent in the time-domain plot are apparent in the shape plot.

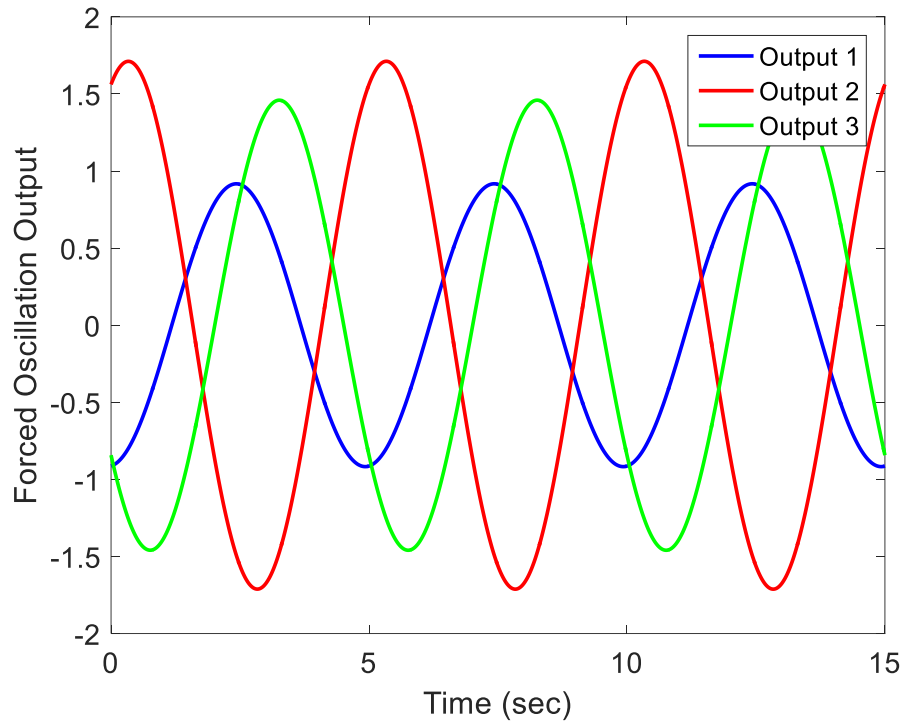


Figure 4-7: Forced oscillation components of the example model outputs in response to a 0.2 Hz sinusoid injected at the model's second input.

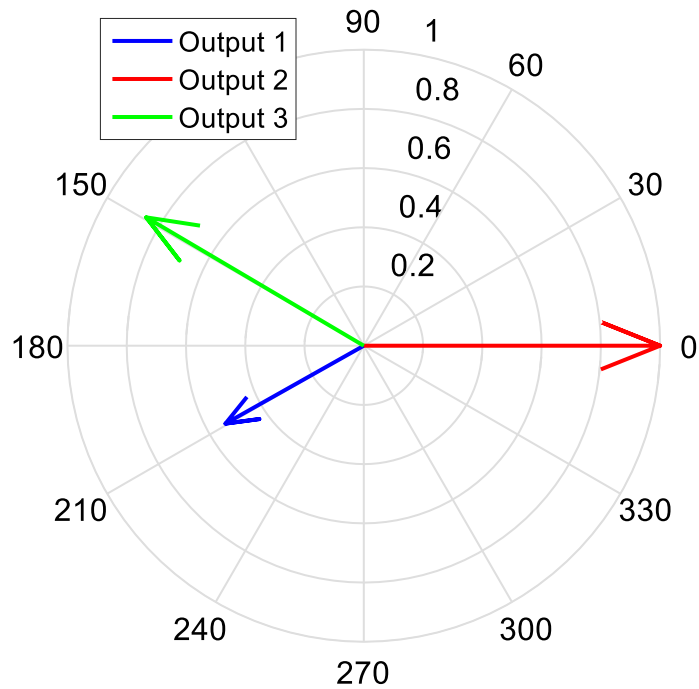


Figure 4-8: Shape of a 0.2 Hz forced oscillation injected at the model's second input.

Next, the same 0.2 Hz sinusoid was applied to the input of the model's third area. The results in Figure 4-9 and Figure 4-10 demonstrate the significant difference in shape that occurs when the input is changed. Likewise, changing the frequency of the input sinusoid to 0.5 Hz leads to a dramatic change in oscillation shape, as depicted in Figure 4-11 and Figure 4-12. In both cases, the shape changes because the system dynamics, which are represented by the model's transfer functions, differ depending on the input location and frequency of the input.

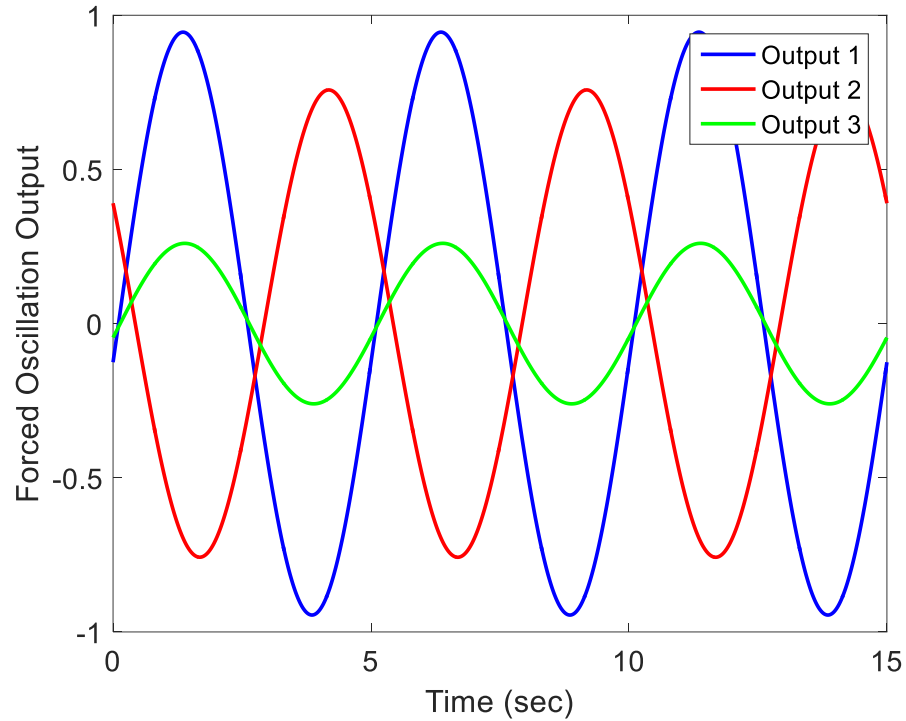


Figure 4-9: Forced oscillation components of the example model outputs in response to a 0.2 Hz sinusoid injected at the model's third input.

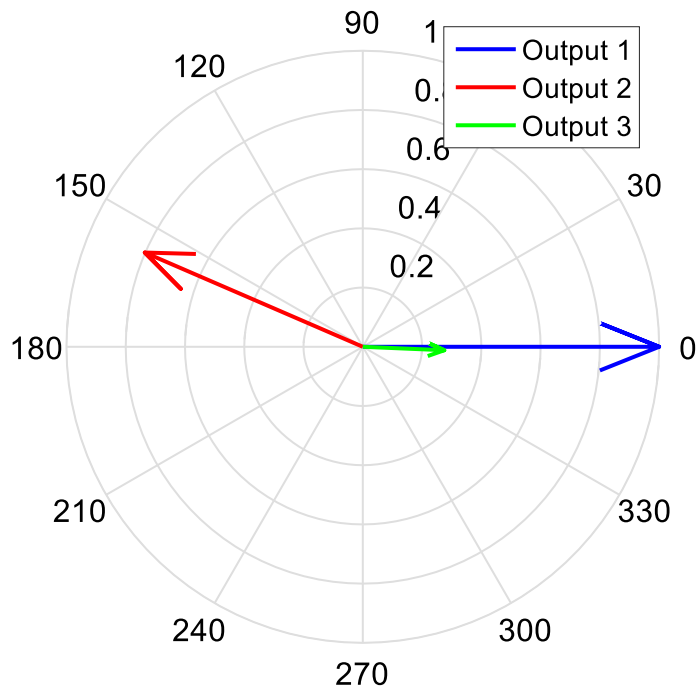


Figure 4-10: Shape of a 0.2 Hz forced oscillation injected at the model's third input.

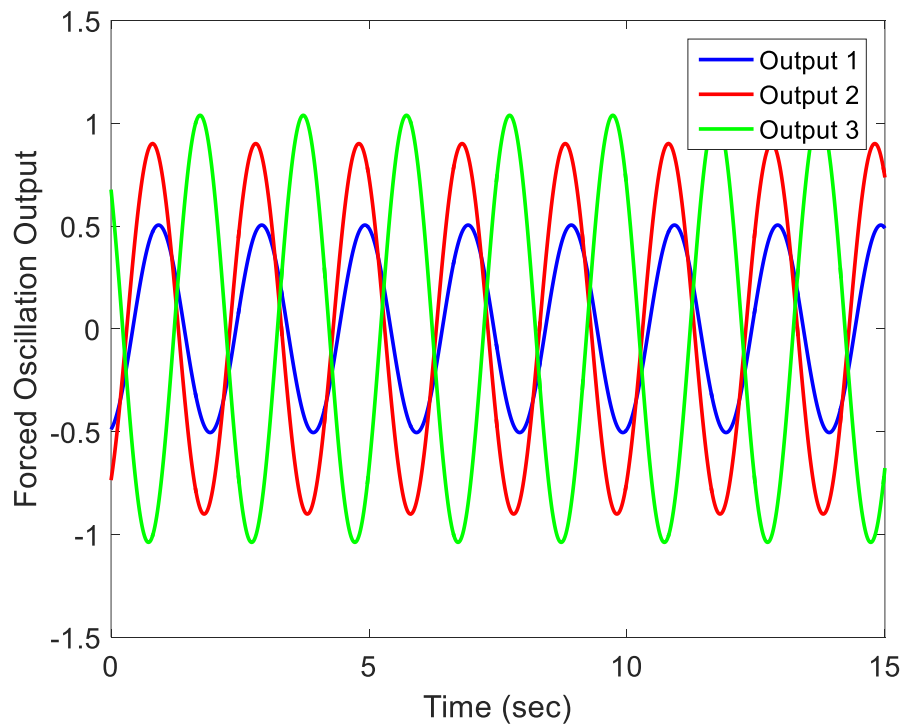


Figure 4-11: Forced oscillation components of the example model outputs in response to a 0.4 Hz sinusoid injected at the model's third input.

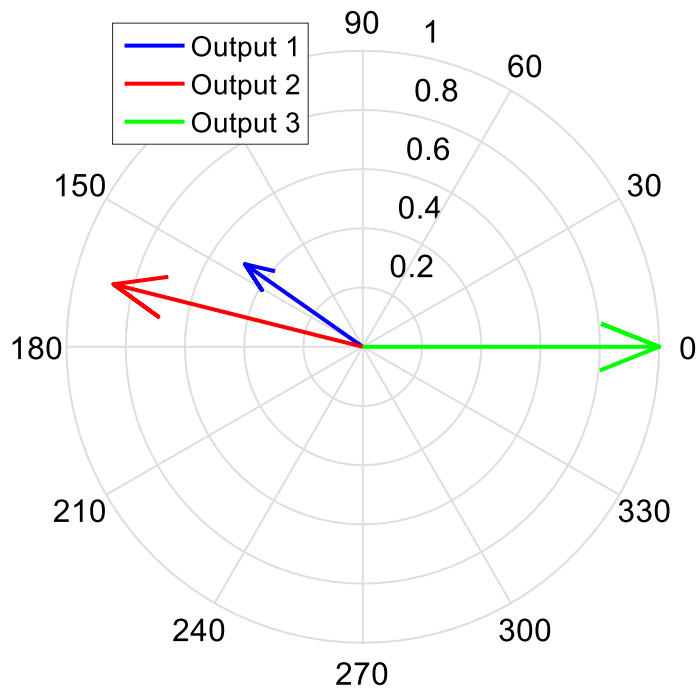


Figure 4-12: Shape of a 0.4 Hz forced oscillation injected at the model's third input.

■

As a consequence of the behavior demonstrated in the previous example, the information provided by a forced oscillation's shape is, in some ways, limited. In particular, Figure 4-9 and Figure 4-10 demonstrate that the oscillation need not be largest in the area it was injected. This behavior has been observed in actual power systems, where a small oscillation injected in one part of the system was observed with significant amplitude in a distant part of the system. Though it is certainly common for a forced oscillation to be largest near its source, it should not be assumed that this is always the case when analyzing measured data.

4.3. Analysis of Forced Responses

The analysis of forced oscillations can generally be broken down into the categories of detection and identification. Detection is necessary because, unlike ambient oscillations, each forced oscillation is only present as long as its driving input is active. Once detected, the parameters of the oscillation, including frequency, amplitude, and phase can be identified. Finally, identifying the source of the oscillation, though often challenging, makes it possible to correct the improper operation leading to the oscillation. In the following two subsections, the aspects of detection and identification of forced oscillations will be discussed.

4.3.1. Detection of Forced Oscillations

Before a forced oscillation can be analyzed or addressed, it must be detected. To do this practically, automated detection methods are needed. These methods can be split into general

categories based on 1) an increase in signal energy, 2) an increase in coherence, and 3) identification of sustained oscillations. These three categories are described in this section, but first performance measures common to all detection algorithms are discussed.

Before proceeding, it should be noted that distinguishing between forced oscillations and sustained, i.e., zero-damped, natural oscillations is a challenge for all methods. In some approaches, the detection algorithm is designed specifically for forced oscillations, while in other cases the determination is made after detection. At present, few analytical methods for distinguishing between forced and natural oscillations have been proposed, so they are not discussed here. The interested reader is referred to (Xie & Trudnowski, 2015) and (Wang & Turitsyn, 2016). Discussion in this section will focus on the overwhelmingly most common case where a sustained oscillation appearing in PMU data is due to a forced, rather than natural, response of the system.

4.3.1.1. Performance Measures for Oscillation Detection

The primary challenge in detecting forced oscillations is achieving an acceptable balance in a method’s performance. The performance of detectors can be evaluated by considering how often the four scenarios in Figure 4-13 occur. Often, mathematical expressions can be developed for the probabilities of detection (quadrant 4), false alarm, and a miss. In the statistical decision theory literature the terms *Type 1 Error* and *Type 2 Error* are often used in place of *False Alarm* and *Miss*, respectively (Kay, 1998).

Ideally, a detection method would always detect an oscillation when it was present (quadrant 4) and would never detect an oscillation when one was not present (quadrant 1). Because power system measurements are composed of more than just forced oscillations, this ideal performance is not possible. Practically, there will always be a risk of failing to detect an oscillation that was present (quadrant 3) and falsely claiming that an oscillation is present when it does not actually exist (quadrant 2). It should be the goal of any detector to mitigate these risks as much as possible, i.e., to reduce the probability of false alarm and the probability of a miss. However, doing so necessarily impacts the probability of detection.

		Oscillation Detected?	
		No	Yes
Oscillation Present?	No	1 Correct Decision	2 False Alarm
	Yes	3 Miss	4 Correct Decision

Figure 4-13: Four possible scenarios when attempting to detect forced oscillations.

Detectors operate by comparing a function of measured data called a *test statistic* to a user-selected value called the *detection threshold*. Detectors use the result of this comparison to determine whether or not an oscillation is likely present. Specific test statistics will be considered in the following subsections. It is important to note the tradeoffs that can be achieved between the four quadrants in Figure 4-13 by adjusting the detection threshold. For example, the detection threshold could be set extremely high to avoid false alarms. However, this will make it very difficult to detect forced oscillations, so many misses will occur. Conversely, the detection threshold could be set extremely low to ensure that all forced oscillations are detected. This approach is equally flawed because it leads to a large number of false alarms. The detection threshold should be set in a manner that balances the probabilities of detection, a miss, and false alarm for a given application.

Though forced oscillations with large amplitudes generally provide the most cause for concern, they are not the only ones present in power systems. For some applications, it may be important to detect low-amplitude forced oscillations as well, but this is challenging due to their low signal-to-noise ratio (SNR). Here the forced oscillation is considered the signal and all other measurement content is considered noise. Reliably detecting low-amplitude forced oscillations requires a lower detection threshold, but because the noise effects are relatively significant, this often leads to a high rate of false alarms.

Comparing two detection methods can involve any number of considerations: required record length, delay before detection, consistent performance across frequencies, processing requirements, etc. However, the probabilities of detection and false alarm are two of the most fundamental and important metrics. When comparing two detectors with identical probabilities of false alarm, the one that achieves a higher probability of detection is deemed more *powerful*. Among the many other considerations listed, it is always desirable to have a more powerful detector because it translates to more events detected and/or fewer false alarms. The specific detectors described in the following sections vary in their power, but their other characteristics make each useful in specific situations.

4.3.1.2. Energy-Based Forced Oscillation Detection

Under ambient conditions, the energy in PMU measurements remains relatively constant from one window of data to the next. However, when a forced oscillation begins, the oscillation's energy is added to the data. Thus, if the energy in two adjacent windows of data is compared and one has significantly more energy, it could signal the presence of a forced oscillation in that window. For example, the energy in each minute of data in Figure 4-1 on page 42 is plotted in Figure 4-14. The red line in the figure indicates a hypothetical detection threshold that could be applied.

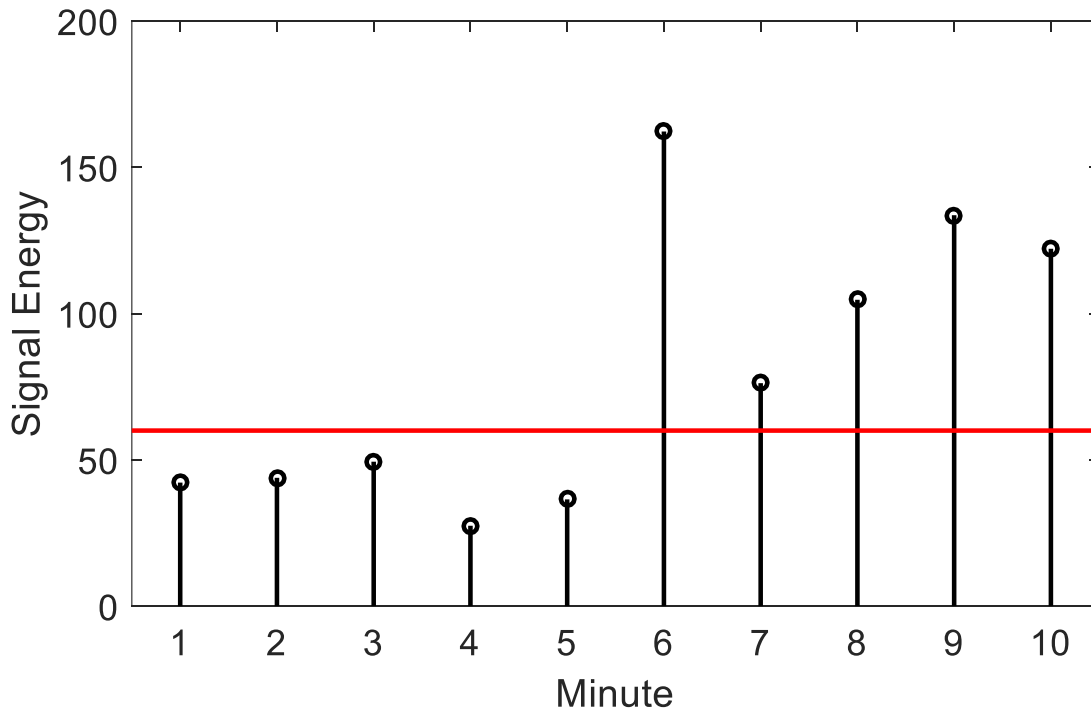


Figure 4-14: Energy in each minute of measured data in Figure 4-1. A hypothetical detection threshold is indicated by the red line.

The example in Figure 4-14 is simple, but it captures the general concept behind a variety of detectors. The concept is refined in (Donnelly, Trudnowski, Colwell, Pierre, & Dosiek, 2015) by applying filters to examine specific frequency bands individually. The practical deployment of this detector is described in (Kosterev, et al., 2016). By essentially narrowing the frequency bands to include individual frequencies, the authors of (Follum & Pierre, 2016) design a detection threshold with associated probabilities of detection and false alarm. Though these specializations become quite involved in the details, the general approach remains straightforward: a significant increase in a PMU measurement’s energy may indicate the onset of a forced oscillation.

4.3.1.3. Coherence-Based Forced Oscillation Detection

As demonstrated in Example 7, a periodic excitation to the system in one area can result in a significant forced oscillation at measured outputs in other areas. Measurements from different areas of the system have more in common while a forced oscillation is present than during ambient conditions. This fact can be exploited to detect the presence of oscillations.

A specific application based on this concept can be found in (Zhou N. , 2013), which proposed examining the spectral coherence between PMU measurements from different areas of a power system. Recall from Section 3.1.3.2 that the spectral coherence provides a frequency dependent measure of how correlated two signals are. During ambient conditions, the spectral coherence between measured data tends to be small, while significant correlation at a specific frequency is indicative of a forced oscillation present in both sets of measurements. Noting that the presence of a forced oscillation causes a signal to remain correlated with itself after a delay, the method was extended in (Zhou & Dagle, 2015) for use with a single channel of data. The multi- and

single-channel approaches both rely on the persistence and periodicity of forced oscillations, characteristics the oscillations inherit from their sources.

4.3.1.4. Detection of Forced Oscillations as General Sustained Oscillations

While recognizing that natural and forced oscillations are distinct in their sources and characteristics, it should also be recognized that they can be detected without distinguishing between them. From (33), it is clear that forced oscillations appear as sinusoids in measured data. If an electromechanical mode is undamped, i.e., $\sigma = 0$, the transient response in (30) will also contain an undamped sinusoid. Thus, methods developed to detect undamped sinusoids can determine when either a forced oscillation or a sustained natural oscillation is present in the system. After the determination is made, the oscillation can be categorized as natural or forced through further examination. Such a method is termed an *oscillation monitor* in (Trudnowski D., Pierre, Donnelly, & Venkatasubramanian, 2015).

4.3.2. Identification of Forced Oscillations

After a forced oscillation has been detected, its parameters can be estimated. From (33), these parameters include each sinusoid's amplitude, frequency, and phase. Combining amplitude and phase estimates from multiple channels leads to an estimate of the forced oscillation's shape. Perhaps the most important parameter from a practical standpoint is the location of the forced oscillation's driving input, which can be used to determine corrective actions. Estimation of each of these parameters will be discussed in this section.

To begin, it should be noted that a forced oscillation's frequency is often estimated upon detection. As an example from methods in Subsections 4.3.1.2 and 4.3.1.3, if the signal energy or the correlation between channels crosses a threshold and peaks at 0.5 Hz, then the frequency of the forced oscillation can immediately be estimated as 0.5 Hz.

If a detection method does not offer frequency estimation, a variety of spectral estimation methods can be implemented. Recall that a signal's spectrum will peak at forced oscillation frequencies due to the signal power concentrated at the frequency. These peaks are apparent in Figure 4-6. Along with non-parametric estimators based on data alone, there are parametric approaches such as the Pisarenko, MUSIC, and ESPRIT methods that are specifically designed to capture sinusoidal signals in noise (Stoica & Moses, 2005). Estimation of a sinusoid's frequency in noise has been well explored and many methods are appropriate. For many applications, simple spectral estimators based on the fast Fourier transform (FFT) are likely sufficient.

The estimation of sinusoidal amplitudes is a similarly well explored area of signal processing. Again, spectral estimation proves a useful tool. The amplitude of a sinusoid with frequency f_{FO} can be estimated as

$$\hat{A} = \sqrt{\hat{\phi}(f_{FO}) \times \frac{f_s}{K}} \quad (34)$$

where $\hat{\phi}(f)$ is the periodogram (25) based on K samples collected at f_s samples per second. In agreement with intuition, this equation demonstrates that the larger a sinusoid's amplitude is, the larger the corresponding peak in the spectrum will be. Similar expressions for amplitude

estimates can be established for other spectral estimators (Zhou & Dagle, 2015). Note, however, that the estimator in (34) does not account for frequency content of the ambient noise comprising the power system's natural response. This issue is addressed in (Follum & Pierre, 2016) with a more detailed amplitude estimator.

Estimation of a forced oscillation's phase is slightly more involved because it cannot rely solely on spectral estimators. The problem is far from insurmountable, though. As with amplitude estimation, the topic of phase estimation for sinusoids has been well explored. Along with non-parametric methods, a straightforward approach would be to fit amplitude and phase terms to a sinusoidal model based on collected measurements. A full description of such an approach can be found in (Kay, 1993), though a phase estimator specific to forced oscillations in power systems has not yet been published.

The reader will note that the descriptions provided in this section are quite brief. This is because while the detection of forced oscillations in power systems offers unique challenges, identification of the oscillation's parameters is relatively straightforward. However, estimation of the final parameter to be considered, the source of the oscillation, is also complicated by the complexity of power systems. Though many papers have been published on the topic, there is not yet widespread agreement about which methods are robust enough to consistently offer an accurate solution. As a result, these methods are not explored in this document.

5. Analysis of Measurements Containing Natural and Forced Responses

Natural and forced responses were considered separately in Sections 3 and 4, but there are several important considerations for analyzing signals containing both types of responses. Because ambient noise is always present, any forced oscillation analysis method must account for this natural response. However, most methods proposed for the analysis of natural responses were not designed to account for forced responses, which are generally temporary. As a result, and as demonstrated in this section, care must be taken when applying analyses specific to natural responses and interpreting their results.

The difficulty introduced by forced oscillations to the attempted analysis of a system's natural response is that they share characteristics with marginally stable natural oscillations. Recall that a system with a zero-damped electromechanical mode will produce sustained oscillations as part of its natural response. It can be difficult to distinguish between these oscillations, which are a serious threat to grid stability, and forced oscillations, which are sustained because of their driving input and do not reflect the grid's stability. For example, consider Figure 5-1, which contains a forced oscillation from 30 to 60 seconds and a natural oscillation from 90 to 120 seconds. The natural oscillation is sustained due to a sudden loss of damping coinciding with the initiating disturbance. The small-signal stability of the system remains unchanged from 0 to 90 seconds, but becomes critical for the last 30 seconds of the simulation. This distinction is difficult to make by examining the time-domain plot, and the same can be true for more rigorous analyses, as detailed in the following example.

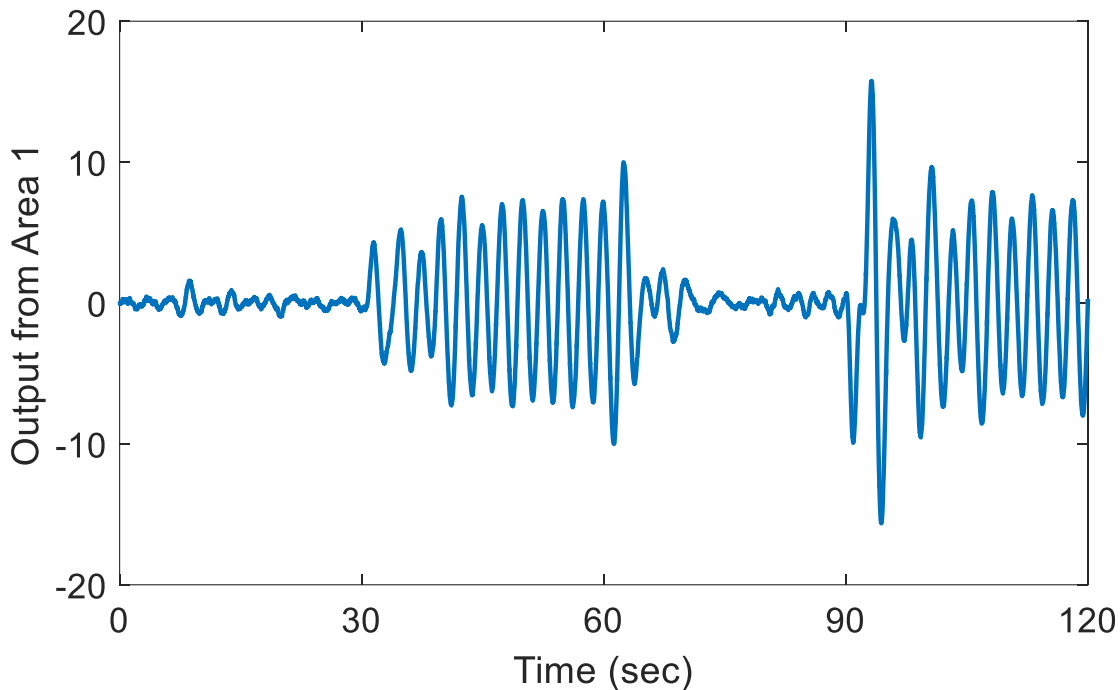


Figure 5-1: Demonstration of the similarity between a forced oscillation (30-60 seconds) and a sustained natural oscillation (90-120 seconds).

Example 8: Impact of a Forced Oscillation on an “Ambient” Data Analysis

This example considers the scenario where the electromechanical modes are to be monitored by analyzing ambient power system measurements with a 10-minute analysis window. The 20-minute set of measurements in Figure 5-2, which was generated using the base test model with modes given in Table 2-1, is considered. For the sake of this example, suppose that the analysis is rerun every 10 minutes to provide updated results. Thus, analyses for minutes 0 through 10 and 10 through 20 will be considered. From the figure, no system changes are apparent, so one would expect similar results for these two analyses. However, a low-amplitude, 0.385 Hz oscillation is present beginning at minute 10 that will significantly impact the results.

Suppose that spectral estimation (see Section 3.1.3.2) is used to provide a rough overview of all the electromechanical modes. The spectral estimate for the first 10-minutes of data in Figure 5-2 based on the commonly used Welch periodogram is presented in Figure 5-3. After 10 minutes, the updated spectral estimate in Figure 5-4 would be obtained. Recall that peaks corresponding to electromechanical modes tend to get taller and narrower as the damping ratio of the corresponding mode declines. Thus, an observer unaware of the forced oscillation’s presence would likely conclude by comparing Figure 5-3 with Figure 5-4 that the damping of the 0.4 Hz mode had dropped. In truth, the system’s modes are unchanged, and the forced oscillation is responsible for the additional frequency content at 0.385 Hz. Forced oscillations can cause misleading results in more rigorous analyses as well.

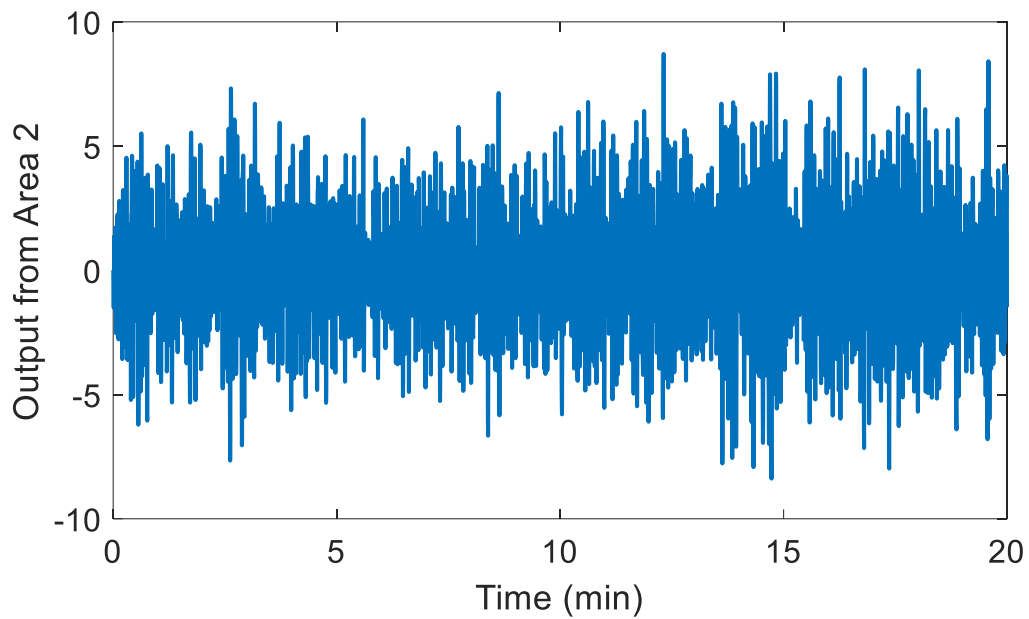


Figure 5-2: Measurements analyzed to monitor the system's electromechanical modes.

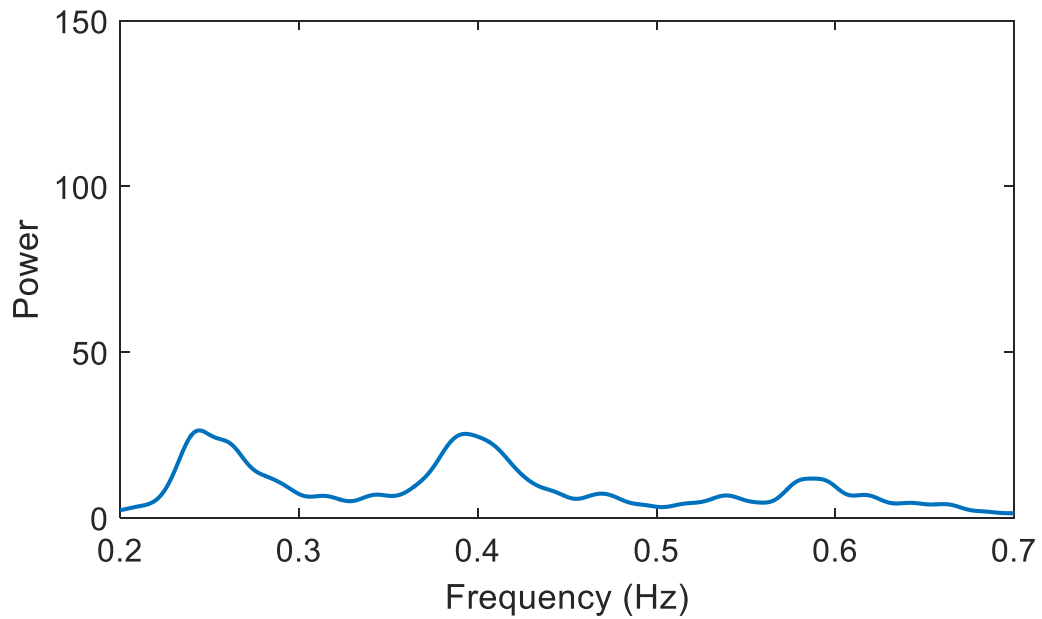


Figure 5-3: Welch periodogram of the first 10 minutes of ambient data in Figure 5-2.

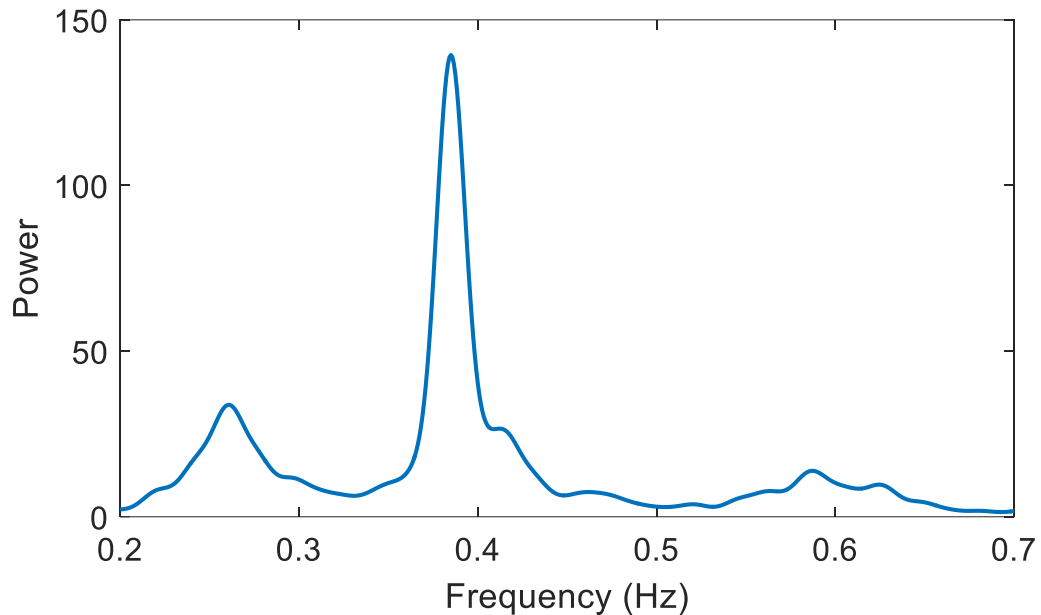


Figure 5-4: Welch periodogram of the second 10 minutes of data in Figure 5-2.

Suppose that the 0.4 Hz mode is also being monitored by fitting an AR model to the data, as was done in Example 1 in Section 3.1.3.1. The ambient data in the first 10 minutes of Figure 5-2 is the same as that used in Example 1, so applying the least-squares algorithm leads to results identical to those given in Example 1. Additionally, the modes are estimated using the second 10 minutes of data in Figure 5-2, which contain the forced oscillation. Mode estimates for each case are presented in Table 5-1. Note that the estimate of the 0.4 Hz mode is much less accurate when the forced oscillation is present. Not coincidentally, the frequency estimate is close to the forced oscillation frequency of 0.385 Hz and the damping ratio is significantly lower than the true value. Unaware of the forced oscillation's presence, an observer would likely conclude that the damping ratio estimate's declining value should be a serious concern, though in reality the system's electromechanical modes were unchanged.

Table 5-1. Actual and estimated mode frequency and damping values for ambient data and data containing a forced oscillation.

Actual Values (Entire 20 Minutes)		Ambient Conditions (First 10 Minutes)		Forced Oscillation Present (Second 10 Minutes)	
Frequency (Hz)	Damping Ratio (%)	Frequency (Hz)	Damping Ratio (%)	Frequency (Hz)	Damping Ratio (%)
0.25	6	0.245	6.65	0.247	7.29
0.4	7	0.401	7.66	0.389	4.17
0.6	6	0.604	6.10	0.605	6.12

The least-squares method is not the only one that is susceptible to bias when forced oscillations with frequencies near electromechanical modes are present in the data. The methods described in Section 3.1.3 are not designed to distinguish between a forced

oscillation and a poorly damped natural oscillation. Without an alternative, they account for the forced oscillation's presence by reporting a natural oscillation with a low damping ratio and a frequency near the frequency of the forced oscillation. This effect is an important consideration when analyzing data that is expected to be ambient but may contain forced oscillations.



The results in the previous example demonstrate the importance of distinguishing between natural and forced oscillations. As emphasized throughout this document, natural oscillations inherit their characteristics (frequency and damping ratio) from the system's dynamics, while forced oscillations inherit their characteristics from the driving input. Forced oscillations are not indicative of problems with the power system's stability, but they can interfere with attempts to monitor the system's stability by estimating its electromechanical modes. A solid understanding of the oscillation sources and characteristics described in this document is vital in applying methods and interpreting results appropriately.

6. Works Cited

- Borden, A. R., Lesieutre, B. C., & Gronquist, J. (2013). Power System Modal Analysis Tool Developed for Industry Use. *North American Power Symposium (NAPS)*. Manhattan, KS.
- Donnelly, M., Trudnowski, D., Colwell, J., Pierre, J., & Dosiek, L. (2015). RMS-Energy Filter Design for Real-Time Oscillation Detection. *2015 IEEE Power & Energy Society General Meeting*, (pp. 1-5). Denver, CO.
- Dosiek, L., & Pierre, J. W. (2013). Estimating electromechanical modes and mode shapes using the multichannel ARMAX model. *Power Systems, IEEE Transactions on*, 28(2), 1950-1959.
- Dosiek, L., Pierre, J. W., Trudnowski, D. J., & Zhou, N. (2009). A Channel Matching Approach for Estimating Electromechanical Mode Shape and Coherence. *IEEE Power & Energy Society General Meeting*. Calgary, AB.
- Dosiek, L., Trudnowski, D. J., & Pierre, J. W. (2008). New Algorithms for Mode Shape Estimation using Measured Data. *IEEE Power & Energy Society General Meeting*. Pittsburgh, PA.
- Dosiek, L., Zhou, N., Pierre, J., Huang, Z., & Trudnowski, D. (2013). Mode Shape Estimation Algorithms Under Ambient Conditions: A Comparative Review. *IEEE Transactions on Power Systems*, 28(2), 779-787.
- Follum, J., & Pierre, J. W. (2016, May). Detection of Periodic Forced Oscillations in Power Systems. *IEEE Transactions on Power Systems*, 31(3), 2423-2433.
- Ghasemi, H., Canizares, C., & Moshref, A. (2006). Oscillatory stability limit prediction using stochastic subspace identification. *Power Systems, IEEE Transactions on*, 21(2), 736-745.
- Hauer, J., Demeure, C., & Scharf, L. (1990). Initial results in Prony analysis of power system response signals. *Power Systems, IEEE Transactions on*, 5(1), 80-89.
- Jingmin, N., Chen, S., & Feng, L. (2011). Estimating the electromechanical oscillation characteristics of power system based on measured ambient data utilizing stochastic subspace method. *Proceedings of the IEEE Power and Energy Society General Meeting*, (pp. 1-7).
- Kamen, E. W., & Heck, B. S. (2007). *Fundamentals of Signals and Systems* (3rd ed.). Upper Saddle River, New Jersey: Pearson Prentice Hall.
- Kamen, E. W., & Heck, B. S. (2007). *Fundamentals of Signals and Systems Using the Web and MATLAB* (3rd ed.). Upper Saddle River, New Jersey: Pearson Prentice Hall.
- Kamwa, I., & Gerin-lajoie, L. (2000). State-space system identification-toward MIMO models for modal analysis and optimization of bulk power systems. *Power Systems, IEEE Transactions on*, 15(1), 326-335.
- Kamwa, I., Grondin, R., Dickinson, E., & Fortin, S. (1993). A minimal realization approach to reduced-order modelling and modal analysis for power system response signals. *Power Systems, IEEE Transactions on*, 8(3), 1020-1029.
- Kay, S. M. (1993). *Fundamentals of Statistical Signal Processing, Volume I: Estimation Theory*. Prentice Hall.
- Kay, S. M. (1998). *Fundamentals of Statistical Signal Processing, Volume 2: Detection theory*. Prentice Hall PTR.
- Kosterev, D., Burns, J., Leitschuh, N., Anasis, J., Donahoo, A., Trudnowski, D., . . . Pierre, J. (2016). Implementation and Operating Experience with Oscillation Detection Application

- at Bonneville Power Administration. *Proceedings of CIGRE 2016 Grid of the Future*. Philadelphia.
- Kundur, P. (1994). *Power System Stability and Control*. New York: McGraw-Hill, Inc.
- Liu, G., & Venkatasubramanian, V. (2008). Oscillation Monitoring from Ambient PMU Measurements by Frequency Domain Decomposition. *IEEE International Symposium on Circuits and Systems*, (pp. 2821-2824).
- Liu, G., Quintero, J., & Venkatasubramanian, V. (2007). Oscillation monitoring system based on wide area synchrophasors in power systems. *Bulk Power System Dynamics and Control – VII. Revitalizing Operational Reliability, 2007 iREP Symposium*. Charleston.
- Ljung, L. (1999). *System Identification: Theory for the User*. Upper Saddle River, NJ: Prentice Hall PTR.
- Myers, R. B., & Trudnowski, D. J. (2013, July). Effects of forced oscillations on spectral-based mode-shape estimation. *2013 IEEE Power Energy Society General Meeting*, (pp. 1-6).
- Pierre, J. W., Trudnowski, D. J., & Donnelly, M. K. (1997). Initial results in electromechanical mode identification from ambient data. *Power Systems, IEEE Transactions on*, 12(3), 1245-1251.
- Pinneilo, J. A., & Van Ness, J. E. (1971). Dynamic response of a large power system to a cyclic load produced by a nuclear accelerator. *Power Apparatus and Systems, IEEE Transactions on*, PAS-90(4), 1856-1862.
- Rao, K. R., & Jenkins, L. (1988). Studies on power systems that are subjected to cyclic loads. *Power Systems, IEEE Transactions on*, 3(1), 31-37.
- Sanchez-Gasca, J., & Chow, J. (1997). Computation of power system low-order models from time domain simulations using a Hankel matrix. *Power Systems, IEEE Transactions on*, 12(4), 1461-1467.
- Silverstein, A. (2015, May). Diagnosing Equipment Health and Mis-operations with PMU Data. *Diagnosing Equipment Health and Mis-operations with PMU Data*. Retrieved from <https://www.naspi.org/documents>
- Stoica, P., & Moses, R. L. (2005). *Spectral Analysis of Signals*. Pearson/Prentice Hall Upper Saddle River, NJ.
- Trudnowski, D. (2008). Estimating Electromechanical Mode Shape from Synchrophasor Measurements. *IEEE Transactions on Power Systems*, 23(3), 1188-1195.
- Trudnowski, D. J., Johnson, J. M., & Hauer, J. F. (1999). Making Prony analysis more accurate using multiple signals. *Power Systems, IEEE Transactions on*, 14(1), 226-231.
- Trudnowski, D. J., Pierre, J. W., Zhou, N., Hauer, J. F., & Parashar, M. (2008). Performance of Three Mode-Meter Block-Processing Algorithms for Automated Dynamic Stability Assessment. *Power Systems, IEEE Transactions on*, 23(2), 680-690.
- Trudnowski, D., Pierre, J., Donnelly, M., & Venkatasubramanian, M. (2015). *Proposed Oscillation Terms*.
- Vanfretti, L., Bengtsson, S., Peric, V. S., & Gjerde, J. O. (2012). Effects of forced oscillations in power system damping estimation. *Proceedings of the IEEE International Workshop on Applied Measurements for Power Systems*, (pp. 1-6).
- Wang, X., & Turitsyn, K. (2016, Sept). Data-Driven Diagnostics of Mechanism and Source of Sustained Oscillations. *IEEE Transactions on Power Systems*, 31(5), 4036-4046.
- Xie, R., & Trudnowski, D. (2015, July). Distinguishing features of natural and forced oscillations. *2015 IEEE Power Energy Society General Meeting*, (pp. 1-5).

- Zhou, N. (2013, July). A coherence method for detecting and analyzing oscillations. *Power and Energy Society General Meeting (PES), 2013 IEEE*, (pp. 1-5).
- Zhou, N., & Dagle, J. (2015, Jan). Initial Results in Using a Self-Coherence Method for Detecting Sustained Oscillations. *Power Systems, IEEE Transactions on*, 30(1), 522-530.
- Zhou, N., Huang, Z., Dosiek, L., Trudnowski, D., & Pierre, J. W. (2009). Electromechanical Mode Shape Estimation based on Transfer Function Identification using PMU Measurements. *IEEE Power & Energy Society General Meeting*. Calgary, AB.
- Zhou, N., Pierre, J., & Wies, R. (2003). Estimation of low-frequency electromechanical modes of power systems from ambient measurements using a subspace method. *Proceedings of the 35th North American Power Symposium*. Tempe.